

Impact and Mitigation of Channel Aging and Electromagnetic Interference on RIS-Assisted Cell-Free Massive MIMO Systems

Jun Qian, *Member, IEEE*, Chi Zhang, *Student Member, IEEE*, Ross Murch, *Fellow, IEEE*, and Khaled B. Letaief, *Fellow, IEEE*

Abstract—Cell-free massive multiple-input multiple-output (MIMO) and reconfigurable intelligent surfaces (RISs) are two potential sixth-generation (6G) technologies. However, channel aging due to user mobility and electromagnetic interference (EMI) impinging on RISs can negatively affect performance. Existing research on RIS-assisted cell-free massive MIMO systems often overlooks these issues. This work focuses on the impact and mitigation of channel aging and EMI on RIS-assisted cell-free massive MIMO systems over spatially correlated channels. To mitigate the degradation caused by these issues, we introduce a novel two-phase channel estimation scheme with large-scale fading coefficient-aided pilot assignment to enhance channel estimation accuracy compared to conventional minimum mean square error estimators. We then develop closed-form expressions for the downlink spectral efficiency (SE) performance and using these, optimize the sum downlink SE with respect to the RIS coefficient matrices. This optimization is accomplished by the projected gradient ascent (GA) algorithm. The results show that our proposed two-phase channel estimation scheme can achieve a nearly 10%-likely SE improvement compared to conventional channel estimation in environments affected by channel aging. A further 10% ~ 15%-likely SE improvement is achieved using the proposed GA algorithm compared to random RIS phases, especially when the number of RISs increases.

Index Terms—Cell-free massive MIMO, channel aging, electromagnetic interference, reconfigurable intelligent surface, spatial correlation, spectral efficiency.

I. INTRODUCTION

IN recent decades, the demand for wireless communication has surged dramatically, reflecting exponential growth. This includes the requirement for higher data rates and widespread connectivity [1]–[4]. The increasing transmission demands have resulted in innovative technologies, such as massive multiple-input multiple-output (MIMO) systems [2], [5]–[7]. However, conventional cellular networks still experience severe inter-cell interference, particularly for cell-edge users limiting overall performance [2], [8].

This work was supported by the Research Grants Council under the Area of Excellence scheme grant AoE/E-601/22-R. This work was partly presented in IEEE International Mediterranean Conference on Communications and Networking, Madrid, Spain, July 2024. (*Corresponding authors: Jun Qian; Chi Zhang.*)

Jun Qian and Chi Zhang are with the Department of Electronic and Computer Engineering, The Hong Kong University of Science and Technology, Hong Kong (e-mail: eejunqian@ust.hk, czhangcc@connect.ust.hk).

Ross Murch and Khaled B. Letaief are with the Department of Electronic and Computer Engineering, The Hong Kong University of Science and Technology, Hong Kong (e-mail: eermurch@ust.hk, eekhaled@ust.hk).

It has been shown that cell-free massive MIMO system can provide effective inter-cell interference mitigation and accomplish quality-of-service (QoS) improvement of cell-edge users [1], [5], [7], [9]. Numerous access points (APs), geographically distributed in the cell-free massive MIMO region without cell boundaries and connected to a central processing unit (CPU), can serve users simultaneously [2], [10]–[12]. APs introduce different contributions to the effective channel gain due to their geographic spread, and conjugate beamforming can satisfy the required performance with computational complexity reduction in a distributed manner [1], [11]. The authors in [7], [10] introduced a large-scale fading decoding (LSFD) process to achieve better uplink spectral efficiency (SE) than the matched filter (MF) in cell-free massive MIMO systems. Also, [13], [14] proposed and utilized the dynamic cooperation cluster concept to introduce scalable cell-free massive MIMO. Despite the above advantages, cell-free massive MIMO still experiences challenges in guaranteeing good service quality under harsh propagation conditions [2], [7]. These challenges require the development of advanced technologies to satisfy the required quality of service.

Reconfigurable intelligent surfaces (RIS) have also attracted great interest in sixth-generation (6G) networks. By smartly shaping electromagnetic-level radio waves without active power amplifiers, RISs introduce a new degree of freedom [7], [15]–[17]. Integrating RISs into wireless networks introduces controllable cascaded links to assist users with undesirable channel propagation conditions [2], [5]. Many important characteristics of RISs have been studied. For example, the authors in [2] introduced an optimal RIS phase shift design for channel estimation error minimisation. [5], [18] proposed a modified channel estimation scheme to achieve better estimation accuracy by introducing higher channel estimation overhead. However, besides the expected signals of the proposed system, uncontrollable wireless signals from outside sources in the physical environment can cause inevitable and non-negligible electromagnetic interference (EMI) or “pollution” impinging on RISs, with an energy proportional to the area of RIS [19]. Since RISs cannot selectively reflect signals, in [19], [20], EMI can also further degrade RIS-assisted system performance. The results in [21] with RIS-assisted ultra-reliable and low-latency wireless communication and [19], [22] with RIS-assisted wireless communication further indicated that the effect of EMI is inevitable and can degrade system performance significantly. As such, the existence of EMI is uncontrollable and non-

negligible in RIS-assisted systems and introduces performance limits [7], [19].

Recently, researchers have focused on integrating cell-free Massive MIMO and RISs to exploit their advantages jointly [23]–[25]. The authors in [24] utilized hybrid active and passive RIS elements in RIS-assisted cell-free massive MIMO. [25] studied the uplink performance of RIS-assisted cell-free massive MIMO with spatial correlation. Channel estimation might be challenging since passive RIS elements make conventional channel estimation infeasible, and increasing RIS elements increases training overhead [17]. Thus, [5], [23] introduced and modified an ON/OFF channel estimation scheme. [26] proposed a two-phase channel estimation scheme with fractional power control-aided pilot assignment to enhance estimation accuracy. Besides [25], the importance of studying the RIS spatial correlation was also indicated in [2], [27]. Assuming EMI to have a uniform distribution across all incident angles, the model for the effect of EMI with RIS spatial correlation has been obtained [7], [19], [20]. This shows that highly correlated RIS elements could introduce severe EMI to degrade RIS-assisted cell-free massive MIMO system performance negatively [7]. However, most works on RIS-assisted cell-free massive MIMO ignore the negative effect of EMI and only consider the system signals [23]–[25]. Inspired by the study of EMI in RIS-assisted systems [19], [21], [22], the authors in [7] first evaluated the uplink performance of RIS-assisted cell-free massive MIMO assisted by RIS with EMI. Since most existing analyses do not apply to RIS-assisted cell-free massive MIMO systems experiencing EMI, limited work has focused on this topic; investigating the performance limits to introduce system design guidelines for RIS-assisted cell-free massive MIMO systems with EMI should be focal.

Furthermore, current works of RIS-assisted cell-free massive MIMO systems are usually based on the block-fading model [2], [5], [7], [8]. However, in practice, users are not static, and the relevant user mobility will introduce continuous channel evolution, which results in the channel aging effect [12], [17]. The work in [12] characterised the channel aging effect on cell-free massive MIMO system performance and compared the performance with the conventional small-cell networks. [16], [17], [28] investigated the system performance of RIS-assisted massive MIMO systems with channel aging effect. Moreover, [17], [28] implemented the RIS coefficient matrix design to maximize the SE performance. However, studying the RIS-assisted cell-free massive MIMO system performance with channel aging remains necessary for real-world mobile transmission scenarios.

To the best of our knowledge, no previous research has examined the combined impact of channel aging and EMI on RIS-assisted cell-free massive MIMO systems, nor has the optimization of the RIS coefficient matrix been investigated in the proposed contexts. However, the interplay between channel aging and EMI is significant and warrants further exploration. Therefore, this paper is the first to develop a system model and perform a performance analysis of spatially correlated RIS-assisted cell-free massive MIMO systems considering both channel aging and EMI. We also investigate the two-phase channel estimation scheme that we have proposed in [26] to

a channel aging-aware environment to mitigate the effect of channel aging and EMI. Our analysis is comprehensive, where conjugate beamforming is applied to the downlink transmission, and downlink fractional power control is introduced to improve downlink SE. To improve system performance, we also propose a RIS coefficient matrix design to maximize the sum downlink SE utilizing the projected gradient ascent (GA) algorithm. The major contributions of this paper include the following:

- We develop a RIS-assisted cell-free massive MIMO system model that accounts for channel aging and EMI, incorporating spatial correlation at both the APs and RISs.
- We introduce an innovative two-phase channel estimation scheme designed to mitigate performance degradation stemming from channel aging and EMI. This approach builds on our previous work [26], adapting it to a channel aging-aware environment. It highlights the advantages of enhanced estimation accuracy, including pilot assignment based on large-scale fading coefficients.
- We evaluate system performance by deriving closed-form expressions for downlink SE. These closed-form expressions enable us to get important insights for system design and performance analysis of the proposed system. Then, motivated by [17], [28], [29], we maximize the sum downlink SE with respect to the design of RIS coefficient matrices based on our derived closed-form SE expressions. We accomplish the maximization problem utilizing the projected GA algorithm.
- We present numerical results to validate our theoretical analyses and offer system design guidelines. Additionally, we examine the impact of channel aging and EMI on downlink SE. The findings demonstrate the effectiveness of the proposed two-phase channel estimation and the optimization algorithm for the RIS coefficient matrix in alleviating performance degradation. Moreover, increasing the number of APs and implementing RISs can further mitigate performance issues, particularly in scenarios with moderate EMI. However, in environments with high EMI, the full benefits of RISs may not be realized.

The remainder of the paper is structured as follows. Section II describes the spatially correlated channel model with channel aging and EMI. Section III introduces our novel two-phase channel estimation scheme, which can mitigate the effects of channel aging and EMI. Section IV derives the achievable downlink SE with fractional power control and optimizes the RIS coefficient matrices to maximize the sum downlink SE. Section V provides numerical results and insights, and Section VI summarizes the current work and proposes future work.

II. SYSTEM MODEL

A. Spatially-Correlated RIS-assisted Channel Model

As shown in Fig. 1, this work considers a RIS-assisted cell-free massive MIMO system operating in a time-division duplex (TDD) mode [26]. M APs serve K single-antenna users simultaneously. All APs, equipped with N antennas per AP, are connected to the CPU via ideal backhaul links [24]. J RISs with L passive reflecting elements per RIS provide communication assistance between APs and users. Note that

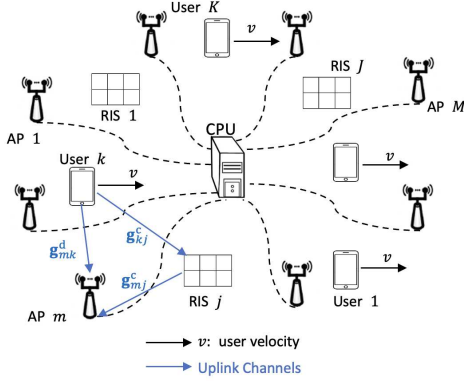


Fig. 1. RIS-assisted cell-free massive MIMO systems with user mobility.

multiple RISs will introduce multi-hop links, namely, the transmission links from APs and reflected by multiple RISs until reaching users [30], and these second-order effects are ignored in this work. Establishing line-of-sight paths is not possible due to user mobility and unknown obstacles and thus, the Rayleigh fading model is considered in this work [16]. Then, the aggregate uplink channel from the k -th user to the m -th AP at time instant n is modelled as [5]

$$\mathbf{g}_{mk}[n] = \mathbf{g}_{mk}^d[n] + \sum_{j=1}^J \mathbf{g}_{mkj}^c[n]. \quad (1)$$

A spatially correlated Rayleigh fading model for the associated channels is considered since multi-antenna APs and multi-element RISs are deployed in our work [16], [17]. First, the direct channel from the k -th user to the m -th AP at time instant n , $\mathbf{g}_{mk}^d[n] \in \mathbb{C}^{N \times 1}$, is expressed as

$$\mathbf{g}_{mk}^d[n] = \sqrt{\beta_{mk}} \mathbf{R}_{mk}^{1/2} \mathbf{v}_{mk}^d[n], \quad (2)$$

where β_{mk} denotes the large-scale fading coefficient between the m -th AP and the k -th user, $\mathbf{R}_{mk} \in \mathbb{C}^{N \times N}$ is the spatial correlation matrix of the m -th AP, $\mathbf{v}_{mk}^d[n] \sim \mathcal{CN}(\mathbf{0}, \mathbf{I}_N)$ refers to the independent fast-fading channel at time instant n .

Then, the cascaded channel from the k -th user to the m -th AP via the j -th RIS at time instant n , $\mathbf{g}_{mkj}^c[n]$, is given by

$$\mathbf{g}_{mkj}^c[n] = \mathbf{g}_{mj}^c[n] \Phi_j[n] \mathbf{g}_{kj}^c[n], \quad (3)$$

where $\mathbf{g}_{mj}^c[n] \in \mathbb{C}^{N \times L}$, the channel from the j -th RIS to the m -th AP based on the classical Kronecker channel model introduced in [31]–[33], is written as

$$\mathbf{g}_{mj}^c[n] = \sqrt{\beta_{mj}} \mathbf{R}_{mj,r}^{1/2} \mathbf{v}_{mj}^c[n] \mathbf{R}_{mj,t}^{1/2}, \quad (4)$$

where β_{mj} represents the large-scale fading coefficient between m -th AP and j -th RIS, the random variables in $\mathbf{v}_{mj}^c[n] \in \mathbb{C}^{N \times L}$ are independent and identically distributed (i.i.d.) and satisfying $\mathcal{N}_c(0, 1)$. $\mathbf{R}_{mj,r} \in \mathbb{C}^{N \times N}$ and $\mathbf{R}_{mj,t} = A_j \mathbf{R}_j \in \mathbb{C}^{L \times L}$ [19], [34] are the one-sided correlations at m -th AP and j -th RIS, respectively. $A_j = d_v d_H$ is the RIS element area; the vertical height and the horizontal width are d_v and d_H , respectively [34]. The (x, y) -th element in \mathbf{R}_j is formulated as [19] [34]

$$[\mathbf{R}_j]_{x,y} = \text{sinc}\left(\frac{2\|\mathbf{u}_x - \mathbf{u}_y\|}{\lambda_c}\right), \quad (5)$$

where $\text{sinc}(x) = \sin(\pi x)/(\pi x)$ and λ_c is the carrier wavelength. Moreover, the position vector follows $\mathbf{u}_y = [0, \text{mod}(y-1, L_h)d_H, [(y-1)/L_h]d_v]^T$, $y \in \{m, n\}$ [19], [25], [34], L_h is the number of column elements and L_v is the number of row elements at each RIS, with $L = L_h \times L_v$.

In this work, we assume that $\mathbf{g}_{mj}^c[n] = \mathbf{g}_{mj}^c$, $n = 1, \dots, \tau_c$, remain constant within the resource block containing τ_c symbols, since only users are movable, while APs and RISs are stationary. The phase shift matrix of j -th RIS is $\Phi_j[n] = \text{diag}(e^{i\phi_{j,11}[n]}, e^{i\phi_{j,22}[n]}, \dots, e^{i\phi_{j,LL}[n]}) \in \mathbb{C}^{L \times L}$, in which $e^{i\phi_{j,ll}[n]}$ is the reflection coefficient of the l -th element in the j -th RIS. Moreover, the induced phase shift is $\phi_{j,ll}[n] \in [0, 2\pi)$ [35]. Since phase shift matrices are controllable, we assume these are pre-assigned and constant as $\Phi_j[n] = \Phi_j$, $n = 1, \dots, \tau_c$ within the resource block. Besides, $\mathbf{g}_{kj}^c[n] \in \mathbb{C}^{L \times 1}$, the channel from the k -th user to the j -th RIS, is given by

$$\mathbf{g}_{kj}^c[n] = \sqrt{\beta_{kj}} \mathbf{R}_{kj}^{1/2} \mathbf{v}_{kj}^c[n]. \quad (6)$$

Similar to (4), β_{kj} is the large-scale fading coefficient between the k -th user and j -th RIS. $\mathbf{v}_{kj}^c[n] \in \mathbb{C}^{L \times 1}$, composed of i.i.d random variables following $\mathcal{CN}(0, 1)$, represents the independent fast-fading channel. $\mathbf{R}_{kj} = A_j \mathbf{R}_j \in \mathbb{C}^{L \times L}$ is the one-sided correlation matrix at the j -th RIS [19], [34]. For the sake of exposition, the covariance matrix of $\mathbf{g}_{mk}[n]$ can be obtained by

$$\begin{aligned} \Delta_{mk} &= \mathbb{E}\{\mathbf{g}_{mk}[n]\mathbf{g}_{mk}[n]^H\} \\ &= \beta_{mk} \mathbf{R}_{mk} + \sum_{j=1}^J \beta_{mj} \beta_{kj} \mathbf{R}_{mj,r} \text{tr}(\mathbf{R}_{mj,t}^{1/2} \Phi_j \mathbf{R}_{kj} \Phi_j^H \mathbf{R}_{mj,t}^{1/2}) \\ &= \beta_{mk} \mathbf{R}_{mk} + \sum_{j=1}^J \beta_{mj} \beta_{kj} \mathbf{R}_{mj,r} \text{tr}(\mathbf{T}_j), \end{aligned} \quad (7)$$

with

$$\mathbf{T}_j = \mathbf{R}_{mj,t}^{1/2} \Phi_j \mathbf{R}_{kj} \Phi_j^H \mathbf{R}_{mj,t}^{1/2} = A_j^2 \mathbf{R}_j^{1/2} \Phi_j \mathbf{R}_j \Phi_j^H \mathbf{R}_j^{1/2}. \quad (8)$$

$$\Delta_{mk}^d = \beta_{mk} \mathbf{R}_{mk}, \quad (9)$$

$$\Delta_{mk}^c = \sum_{j=1}^J \beta_{mj} \beta_{kj} \mathbf{R}_{mj,r} \text{tr}(\mathbf{T}_j). \quad (10)$$

B. Electromagnetic Interference Model

According to [7], [19], [20], uncontrollable external sources can generate the superposition of a continuum of incoming plane waves and result in non-negligible EMI that degrades system performance. The effect of EMI can be modelled by using the RIS correlation matrix under isotropic conditions [2], [7], [19]. Then, the EMI impinging on the j -th RIS can be given by

$$\mathbf{n}_j \sim \mathcal{CN}(0, A_j \sigma_j^2 \mathbf{R}_j), \quad (11)$$

where σ_j^2 is the EMI power at the j -th RIS. In this work, we introduce a modified EMI power expression referring to [7], [19], so that it is scalable and suitable for analysis

$$\sigma_j^2 = \sqrt{\frac{p_u p_d \sum_{m=1}^M \beta_{mj} \sum_{k=1}^K \beta_{kj}}{MK \zeta_j^2}}, \quad (12)$$

where p_u and p_d represent the respective uplink and downlink transmit power. The received signal power divided by the EMI power represents the ratio ζ_j at the j -th RIS [7], [19]. For simplicity, we assume $\zeta_j = \zeta$, $\forall j$.

C. Channel Aging

In general, user mobility generates relative movement between the users and APs/RISs, leading to a Doppler shift that changes the AP-user and RIS-user channels over time. This phenomenon is introduced as the channel aging effect [12], [17]. As such, the channel coefficients within each symbol remain constant and change from symbol to symbol. Unlike the block-fading model, this channel-varying assumption is commonly used in works concerning the channel aging effect [12], [17], [24]. Mathematically, the summation of the corresponding initial states $\mathbf{g}_{mk}[0]$ and the evolution component can model the aggregate uplink channel $\mathbf{g}_{mk}[n]$, which can be expressed as [12], [18], [36], [37]

$$\mathbf{g}_{mk}[n] = \rho_k[n]\mathbf{g}_{mk}[0] + \bar{\rho}_k[n]\mathbf{e}_{mk}[n], \quad (13)$$

where $\rho_k[n] = J_0(2\pi f_{D,k}T_s n)$ represents the temporal correlation coefficient combating the channel aging effect for the k -th user at time instant n with $\bar{\rho}_k[n] = \sqrt{1 - \rho_k^2[n]}$ [18], [37], [38]. $J_0(\cdot)$ denotes the zero-order Bessel function of the first kind, $f_{D,k} = \frac{v_k f_c}{c}$ is the k -th user's Doppler shift, and T_s is the time instant length. Moreover, v_k is the k -th user velocity, $c = 3 \times 10^8$ m/s is the speed of light, and f_c is the carrier frequency. We can see that a higher user velocity or delay can decrease $\rho_k[n]$. Furthermore, the model in (13) depends on its initial state at time instant 0, $\mathbf{g}_{mk}[0]$, to match with the statistics of Jakes' model [16], [17] [39].

According to (1), the channel coefficients $\mathbf{g}_{mk}^d[n]$ and $\mathbf{g}_{mkj}^c[n]$ can be expressed by their respective initial states $\mathbf{g}_{mk}^d[0]$, $\mathbf{g}_{mkj}^c[0]$ and the perturbation terms [16]. Then, we can obtain $\mathbf{g}_{mk}[n]$ at time instant n as

$$\begin{aligned} \mathbf{g}_{mk}[n] &= \rho_k[n]\mathbf{g}_{mk}^d[0] + \bar{\rho}_k[n]\mathbf{e}_{mk}^d[n] \\ &+ \sum_{j=1}^J \rho_k[n]\mathbf{g}_{mkj}^c[0] + \sum_{j=1}^J \bar{\rho}_k[n]\mathbf{e}_{mkj}^c[n], \end{aligned} \quad (14)$$

where $\mathbf{e}_{mk}^d[n]$ and $\mathbf{e}_{mkj}^c[n]$ are the independent AP-user and RIS-AP-user innovation component with $\mathbf{e}_{mk}^d[n] \sim \mathcal{CN}(\mathbf{0}, \beta_{mk}\mathbf{R}_{mk})$ and $\mathbf{e}_{mkj}^c[n] = \mathbf{g}_{mj}^c \theta_j[n] \mathbf{e}_{kj}^c[n] \sim \mathcal{CN}(\mathbf{0}, \beta_{mj}\beta_{kj}\mathbf{R}_{mj}, \text{tr}(\mathbf{T}_j))$, where $\mathbf{e}_{kj}^c[n] \sim \mathcal{CN}(\mathbf{0}, \beta_{kj}A_j\mathbf{R}_j)$, respectively.

III. NOVEL TWO-PHASE CHANNEL ESTIMATION

Usually, users first send the pilots to APs, which adopt the minimum mean square error (MMSE) estimate to acquire the uplink channel state information (CSI) [5]. Then, the obtained uplink CSI will be applied to introduce the channel distribution of other time instants with the temporal correlation coefficients across different time instants [16], [40], [41]. To improve the channel estimation accuracy, we extend our novel two-phase channel estimation scheme [26] to enhance channel estimation accuracy and mitigate the effect of channel aging and EMI. Compared with the conventional MMSE estimation scheme, which simultaneously estimates the aggregate channels (both direct and RIS-assisted channels) and might cause poor channel estimation accuracy [5], [16], [23], [41], our proposed scheme divides the channel estimation phase into two sub-phases, each taking τ_p samples. The two sub-phases estimate the direct and RIS-assisted channels in sequence, and

each sub-phase involves fractional power control-aided pilot assignment for channel estimation improvement.

A. Large-Scale Fading Coefficient-based Pilot Assignment

In the uplink channel estimation phase, we utilize the user's large-scale fading coefficients to introduce an appropriate pilot assignment to reduce the pilot contamination and guarantee a certain QoS for all users [27]. First, for the x -th sub-phase, the $m_k^{\max,x}$ -th AP with the largest Δ_{mk}^x can be chosen as the prime AP of the k -th user,

$$m_k^{\max,x} = \arg \max_{m \in \{1, \dots, M\}} \text{tr}(\Delta_{mk}^x), \quad (15)$$

where $x = d, c$ denotes the ongoing sub-phase and subsequently, the $m_k^{\max,x}$ -th AP determines the pilot sequence allocation of φ_k to the k -th user during the relevant sub-phase. To mitigate pilot contamination, the pilot sequence with index $t_k^x = k$ is allocated to the k -th user when $k < \tau_p$, and when $k > \tau_p$, t_k follows

$$t_k^x = \arg \min_{t \in \{1, 2, \dots, \tau_p\}} \sum_{i \in \mathcal{S}_t} \text{tr}(\Delta_{m_i^{\max,x,i}}^x), \quad (16)$$

where \mathcal{S}_t is the set of users assigned with pilot sequence t , and \mathcal{S}_t will be updated when each k -th user ($k > \tau_p$) is assigned with its own pilot sequence t_k^x based on (16). With the help of the pilot assignment, we can determine \mathcal{P}_k^x ($x = d, c$, $k = 1, \dots, K$), as the set of users sharing the same pilot sequence including the k -th user itself in the ongoing x -th sub-phase.

B. Uplink Channel Estimation

We define the pilot sequence allocated to the k -th user as $\varphi_k \in \mathbb{C}^{\tau_p \times 1}$ with $\varphi_k^H \varphi_k = 1, \forall k$, where τ_p is the pilot length. Usually, the coherence interval length τ_c is much larger than τ_p to guarantee the transmission efficiency, implying that $K > \tau_p$ [2], [7]. Different users will share the same pilot sequence in this case, leading to pilot contamination [42]. According to the pilot assignment procedure, \mathcal{P}_k^x is the set of users sharing the same pilot in the ongoing sub-phase satisfying $\varphi_k^H \varphi_{k'} = 1, \forall k' \in \mathcal{P}_k^x$, inevitably.

1) *Direct channel estimation sub-phase*: All RIS elements are OFF within the current sub-phase. Then, all users transmit their pilots to the APs to estimate the direct channel. τ_p pre-defined mutually orthogonal pilot sequences are used in this sub-phase. Referring to the channel estimation model experiencing channel aging in [12], the pilot sequence t is sent only at time instant t within the sub-phase to maintain the orthogonality between the pilots with channel aging. $t_k^d \in 1, \dots, \tau_p$ is the time instant index assigned to the k -th user, and the other users in the pre-defined set \mathcal{P}_k^d share the same pilot transmission time instant, namely, $\mathcal{P}_k^d = \{k' : t_{k'}^d = t_k^d\} \subset \{1, \dots, K\}$. The pilot signal, $\mathbf{Y}_{m,p}^d[t_k] \in \mathbb{C}^{N \times \tau_p}$, received at the m -th AP at the t_k^d -th time instant is formulated as

$$\mathbf{Y}_{m,p}^d[t_k^d] = \sum_{k'=1}^K \sqrt{p_p} \mathbf{g}_{mk'}^d[t_k^d] \varphi_{k'}^H + \mathbf{W}_{m,p}^d[t_k^d], \quad (17)$$

where p_p is the pilot power for each user. $\mathbf{W}_{m,p}^d[t_k^d]$ is the additive white Gaussian noise (AWGN) at the m -th AP during this sub-phase with v -th column satisfying $[\mathbf{W}_{m,p}^d[t_k^d]]_v \sim \mathcal{CN}(\mathbf{0}, \sigma^2 \mathbf{I}_N)$, where σ^2 is the noise power. We focus on the

channel estimates at λ -th time instant in the following, where $\lambda = 2\tau_p + 1$. Then, these estimates will be treated as the initial states to generate the other time instants' channel estimates. We can obtain the effective channel at the t_k^d -th time instant based on the channel at the λ -th time instant as

$$\mathbf{g}_{mk'}^d[t_k^d] = \rho_{k'}[\lambda - t_k^d]\mathbf{g}_{mk'}^d[\lambda] + \bar{\rho}_{k'}[\lambda - t_k^d]\mathbf{e}_{mk'}^d[t_k^d]. \quad (18)$$

By projecting $\mathbf{Y}_{m,p}^d[t_k^d]$ on $\boldsymbol{\varphi}_k$, we can obtain

$$\begin{aligned} \mathbf{y}_{mk,p}^d[t_k^d] &= \sum_{k'=1}^K \sqrt{p_p}\mathbf{g}_{mk'}^d[t_k^d]\boldsymbol{\varphi}_k^H\boldsymbol{\varphi}_k + \mathbf{W}_{m,p}^d[t_k^d]\boldsymbol{\varphi}_k \\ &= \sum_{k' \in \mathcal{P}_k^d} \sqrt{p_p}\mathbf{g}_{mk'}^d[t_k^d] + \mathbf{W}_{m,p}^d[t_k^d]\boldsymbol{\varphi}_k. \end{aligned} \quad (19)$$

Given (19), the MMSE estimation of $\mathbf{g}_{mk}^d[\lambda]$ is given by

$$\hat{\mathbf{g}}_{mk}^d[\lambda] = \mathbf{R}_{mk}^d(\boldsymbol{\Psi}_{mk}^d)^{-1}\mathbf{y}_{mk,p}^d[t_k^d], \quad (20)$$

where

$$\mathbf{R}_{mk}^d = \sqrt{p_p}\rho_k[\lambda - t_k^d]\beta_{mk}\mathbf{R}_{mk}, \quad (21)$$

$$\boldsymbol{\Psi}_{mk}^d = \sum_{k' \in \mathcal{P}_k^d} p_p\beta_{mk'}^d\mathbf{R}_{mk'} + \sigma^2\mathbf{I}_N. \quad (22)$$

2) *RIS-assisted channel estimation sub-phase*: All RIS elements are ON within this sub-phase. Similarly, the pre-defined τ_p pilot sequences are applied, and the pilot sequence t is sent only at time instant $t + \tau_p$ during the current sub-phase [12]. $t_k^c \in \{\tau_p, \dots, 2\tau_p\}$ is the pilot sequence assigned to users utilizing the same time instant as the k -th user, follows $\mathcal{P}_k^c = \{k' : t_{k'}^c = t_k^c\} \subset \{1, \dots, K\}$. For simplicity of notation, $t_k^c = \tau_p + t_k^c \in \{\tau_p + 1, \dots, 2\tau_p\}$ represents the relevant time instant index during the current sub-phase. As such, $\mathbf{Y}_{m,p}[t_k] \in \mathbb{C}^{N \times \tau_p}$, the received pilot signal at the m -th AP, can be modelled as

$$\begin{aligned} \mathbf{Y}_{m,p}[t_k^c] &= \sum_{k'=1}^K \sqrt{p_p}(\mathbf{g}_{mk'}^d[t_k^c] + \sum_{j=1}^J \mathbf{g}_{mk'j}^c[t_k^c])\boldsymbol{\varphi}_k^H \\ &\quad + \sum_{j=1}^J \mathbf{g}_{mj}^c\boldsymbol{\Phi}_j\mathbf{N}_j[t_k^c] + \mathbf{W}_{m,p}^c[t_k^c], \end{aligned} \quad (23)$$

where $\mathbf{W}_{m,j,p}^c[t_k^c]$ is the AWGN matrix in this sub-phase with $[\mathbf{W}_{m,p}^c[t_k^c]]_v \sim \mathcal{CN}(\mathbf{0}, \sigma^2\mathbf{I}_N)$. Moreover, $\mathbf{N}_j[t_k^c] \in \mathbb{C}^{L \times \tau_p}$ is the EMI of the j -th RIS with v -th column satisfying $[\mathbf{N}_j[t_k^c]]_v \sim \mathcal{CN}(0, A_j\sigma_j^2\mathbf{R}_j)$. Since the direct link has already been estimated in the first sub-phase and $\hat{\mathbf{g}}_{mk}^d[\lambda]$ is known at the m -th AP. We consider the perfect subtraction of $\mathbf{Y}_{m,p}^d[t_k^c]$ from $\mathbf{Y}_{m,p}[t_k^c]$ in the this work, the imperfect subtraction will be left for future work. Then, we can obtain

$$\begin{aligned} \mathbf{Y}_{m,p}[t_k^c] &= \sum_{k'=1}^K \sum_{j=1}^J \sqrt{p_p}\mathbf{g}_{mk'j}^c[t_k^c]\boldsymbol{\varphi}_k^H \\ &\quad + \sum_{j=1}^J \mathbf{g}_{mj}^c\boldsymbol{\Phi}_j\mathbf{N}_j[t_k^c] + \mathbf{W}_{m,j,p}^c[t_k^c], \end{aligned} \quad (24)$$

similar to (18), the effective channel at the t_k^c -th time instant based on the channel at the λ -th time instant is expressed as

$$\begin{aligned} \mathbf{g}_{mk'}^c[t_k^c] &= \rho_{k'}[\lambda - t_k^c] \sum_{j=1}^J \mathbf{g}_{mk'j}^c[\lambda] \\ &\quad + \bar{\rho}_{k'}[\lambda - t_k^c] \sum_{j=1}^J \mathbf{e}_{mk'j}^c[t_k^c]. \end{aligned} \quad (25)$$

The projection of $\mathbf{Y}_{m,p}[t_k^c]$ on $\boldsymbol{\varphi}_k$ can be formulated as

$$\begin{aligned} \mathbf{y}_{mk,p}[t_k^c] &= \sum_{k' \in \mathcal{P}_k^c} \sum_{j=1}^J \sqrt{p_p}\mathbf{g}_{mk'j}^c[t_k^c] \\ &\quad + \sum_{j=1}^J \mathbf{g}_{mj}^c\boldsymbol{\Phi}_j\mathbf{N}_j[t_k^c]\boldsymbol{\varphi}_k + \mathbf{W}_{m,p}^c[t_k^c]\boldsymbol{\varphi}_k. \end{aligned} \quad (26)$$

Given (26), the MMSE of $\mathbf{g}_{mk}^c[\lambda] = \sum_{j=1}^J \mathbf{g}_{mkj}^c[\lambda]$ is defined as

$$\hat{\mathbf{g}}_{mk}^c[\lambda] = \mathbf{R}_{mk}^c(\boldsymbol{\Psi}_{mk}^c)^{-1}\mathbf{y}_{mk,p}^c[t_k^c], \quad (27)$$

where

$$\mathbf{R}_{mk}^c = \sqrt{p_p}\rho_k[\lambda - t_k^c] \sum_{j=1}^J \beta_{mj}\beta_{kj}\text{tr}(\mathbf{T}_j)\mathbf{R}_{mj,r}, \quad (28)$$

$$\boldsymbol{\Psi}_{mk}^c = \sum_{k' \in \mathcal{P}_k^c} p_p\Delta_{mk'}^c + \sum_{j=1}^J \beta_{mj}\sigma_j^2\text{tr}(\mathbf{T}_j)\mathbf{R}_{mj,r} + \sigma^2\mathbf{I}_N. \quad (29)$$

Based on the above, the sum of the direct channel estimate and cascaded RIS-assisted channel estimates introduces the MMSE channel estimate $\hat{\mathbf{g}}_{mk}[\lambda]$, which can be formulated as

$$\hat{\mathbf{g}}_{mk}[\lambda] = \hat{\mathbf{g}}_{mk}^d[\lambda] + \hat{\mathbf{g}}_{mk}^c[\lambda]. \quad (30)$$

The channel estimate $\hat{\mathbf{g}}_{mk}[\lambda]$ and the channel estimation error $\tilde{\mathbf{g}}_{mk}[\lambda] = \mathbf{g}_{mk}[\lambda] - \hat{\mathbf{g}}_{mk}[\lambda]$ are distributed as $\mathcal{CN}(\mathbf{0}, \mathbf{Q}_{mk}^d + \mathbf{Q}_{mk}^c)$ and $\mathcal{CN}(\mathbf{0}, \Delta_{mk} - \mathbf{Q}_{mk}^d - \mathbf{Q}_{mk}^c)$, respectively, with $\mathbf{Q}_{mk}^x = \mathbf{R}_{mk}^x(\mathbf{R}_{mk}^x(\boldsymbol{\Psi}_{mk}^x)^{-1})^H$, $x \in \{d, c\}$.

Moreover, to study the channel estimation accuracy, the normalised mean square error (NMSE) of the channel estimation is modelled as [5], [39]

$$\text{NMSE} = \frac{\sum_{m,k} \mathbb{E}\{\|\tilde{\mathbf{g}}_{mk}[\lambda]\|^2\}}{\sum_{m,k} \mathbb{E}\{\|\mathbf{g}_{mk}[\lambda]\|^2\}} = \frac{\sum_{m,k} \text{tr}(\Delta_{mk} - \mathbf{Q}_{mk}^d - \mathbf{Q}_{mk}^c)}{\sum_{m,k} \text{tr}(\Delta_{mk})}. \quad (31)$$

In this case, $\mathbf{g}_{mk}[n]$, taking the joint channel aging and channel estimation error into consideration, can be formulated as [16], [39]

$$\begin{aligned} \mathbf{g}_{mk}[n] &= \rho_k[n - \lambda](\hat{\mathbf{g}}_{mk}^d[\lambda] + \tilde{\mathbf{g}}_{mk}^d[\lambda]) + \bar{\rho}_k[n - \lambda]\mathbf{e}_{mk}^d[n] \\ &\quad + \rho_k[n - \lambda](\hat{\mathbf{g}}_{mk}^c[\lambda] + \tilde{\mathbf{g}}_{mk}^c[\lambda]) + \sum_{j=1}^J \bar{\rho}_k[n - \lambda]\mathbf{e}_{mkj}^c[n]. \end{aligned} \quad (32)$$

IV. DOWNLINK SE ANALYSIS AND SUM SE MAXIMIZATION

This section analyzes the downlink data transmission affected by channel aging and EMI. After uplink channel estimation, $\tau_c - 2\tau_p$ time instants are adopted for the downlink transmission. We derive novel downlink SE closed-form expressions and utilize downlink fractional power control to evaluate system performance. We then find the RIS coefficient matrix design to maximize the sum downlink SE.

A. Downlink Data Transmission

The downlink data transmission from all APs to all users is composed of a broadcast channel utilizing the beamforming vector $\mathbf{f}_{mk}[n] \in \mathbb{C}^{N \times 1}$ at the m -th AP [17]. We treat the uplink channel transpose as the downlink channel based on the channel reciprocity characteristic of TDD operation. [18], [39]. As such, the transmit signal at time instant n from the m -th AP is formulated as

$$\mathbf{x}_m[n] = \sqrt{p_d} \sum_{k=1}^K \mathbf{f}_{mk}[n] \sqrt{\eta_{mk}}q_k[n], \quad (33)$$

where p_d denotes the downlink transmit power at APs, η_{mk} is downlink power control coefficients with $\mathbb{E}\{|\mathbf{x}_m[n]|^2\} \leq p_d$. $q_k[n] \sim \mathcal{CN}(0, 1)$ is the signal sent to the k -th user, same for

$$\begin{aligned}
r_k[n] &= \sum_{m=1}^M \mathbf{g}_{mk}^T[n] \mathbf{x}_m[n] + \sum_{j=1}^J (\mathbf{g}_{kj}^c[n])^T \mathbf{\Phi}_j^T \mathbf{n}_j[n] + w_k[n] \\
&= \sum_{m=1}^M \sum_{k'=1}^K \mathbf{g}_{mk}^T[n] \sqrt{\rho_d} \hat{\mathbf{g}}_{mk'}^*[\lambda] \sqrt{\eta_{mk'}} q_{k'}[n] + \sum_{j=1}^J (\mathbf{g}_{kj}^c[n])^T \mathbf{\Phi}_j^T \mathbf{n}_j[n] + w_k[n] \\
&= \underbrace{\sqrt{\rho_d} \rho_k [n - \lambda] \sum_{m=1}^M \mathbb{E} \left\{ \mathbf{g}_{mk}^T[\lambda] \hat{\mathbf{g}}_{mk}^*[\lambda] \right\} \sqrt{\eta_{mk}} q_k[n]}_{\text{DS}_k[n]} + \underbrace{\sqrt{\rho_d} \rho_k [n - \lambda] \sum_{m=1}^M \left(\mathbf{g}_{mk}^T[\lambda] \hat{\mathbf{g}}_{mk}^*[\lambda] - \mathbb{E} \left\{ \mathbf{g}_{mk}^T[\lambda] \hat{\mathbf{g}}_{mk}^*[\lambda] \right\} \right) \sqrt{\eta_{mk}} q_k[n]}_{\text{BU}_k[n]} \\
&\quad + \underbrace{\sqrt{\rho_d} \bar{\rho}_k [n - \lambda] \sum_{m=1}^M \mathbf{e}_{mk}^T[n] \hat{\mathbf{g}}_{mk}^*[\lambda] \sqrt{\eta_{mk}} q_k[n]}_{\text{CA}_k[n]} + \sum_{k' \neq k}^K \underbrace{\sqrt{\rho_d} \sum_{m=1}^M \mathbf{g}_{mk}^T[n] \hat{\mathbf{g}}_{mk'}^*[\lambda] \sqrt{\eta_{mk'}} q_{k'}[n]}_{\text{UI}_{kk'}[n]} + \underbrace{\sum_{j=1}^J (\mathbf{\Phi}_j \mathbf{g}_{kj}^c[n])^T \mathbf{n}_j[n]}_{\text{EMI}_k[n]} + \underbrace{w_k[n]}_{\text{NS}_k[n]}, \tag{34}
\end{aligned}$$

$$S_k[n] = p_d \rho_k^2 [n - \lambda] \left| \sum_{m=1}^M \sqrt{\eta_{mk}} \mathbb{E} \left\{ \mathbf{g}_{mk}^T[\lambda] \hat{\mathbf{g}}_{mk}^*[\lambda] \right\} \right|^2 = p_d \rho_k^2 [n - \lambda] \left| \sum_{m=1}^M \sqrt{\eta_{mk}} \text{tr}(\mathbf{Q}_{mk}^d + \mathbf{Q}_{mk}^c) \right|^2, \tag{38}$$

$$\begin{aligned}
I_k[n] &= p_d \sum_{k'=1}^K \mathbb{E} \left\{ \left| \sum_{m=1}^M \sqrt{\eta_{mk'}} \mathbf{g}_{mk'}^T[n] \hat{\mathbf{g}}_{mk'}^*[\lambda] \right|^2 \right\} - S_k[n] + \mathbb{E} \left\{ \left| \sum_{j=1}^J (\mathbf{\Phi}_j \mathbf{g}_{kj}^c[n])^T \mathbf{n}_j[n] \right|^2 \right\} + \sigma^2 \\
&= p_d \sum_{k'=1}^K \mathbb{E} \left\{ \left| \sum_{m=1}^M \sqrt{\eta_{mk'}} \mathbf{g}_{mk'}^T[n] \hat{\mathbf{g}}_{mk'}^*[\lambda] \right|^2 \right\} - S_k[n] + \sum_{j=1}^J \beta_{kj} \sigma_j^2 \text{tr}(\mathbf{T}_j) + \sigma^2. \tag{39}
\end{aligned}$$

all APs. Conjugate beamforming at APs is selected, namely, $\mathbf{f}_{mk}[n] = \hat{\mathbf{g}}_{mk}^*[\lambda]$ for $\lambda \leq n \leq \tau_c$. Then, (34) describes the k -th user's received signal at the top of the next page. $\mathbf{n}_j[n] \sim \mathcal{CN}(0, A_j \sigma_j^2 \mathbf{R}_j)$ is the EMI of the j -th RIS, $w_k[n] \sim \mathcal{CN}(0, \sigma^2)$ is the AWGN at the k -th user at time instant n .

Motivated by [17], [43], we propose a fractional power control scheme including statistical channel information and generate the fractional power control coefficients as

$$\eta_{mk} = \left(\sum_{k'=1}^K \text{tr}(\mathbf{Q}_{mk'}^d + \mathbf{Q}_{mk'}^c) \right)^{-1}, \quad \forall k, \forall m. \tag{35}$$

B. Performance Analysis and Closed-form SE Derivations

According to (34), the downlink achievable SE of the k -th user is lower bounded by [5], [12]

$$\text{SE}_k = \frac{1}{\tau_c} \sum_{n=\lambda}^{\tau_c} \log_2(1 + \text{SINR}_k[n]), \tag{36}$$

where $\text{SINR}_k[n]$ is the effective signal-to-interference-plus-noise ratio (SINR) at time instant n can be expressed as,

$$\text{SINR}_k[n] = \frac{S_k[n]}{I_k[n]}, \tag{37}$$

where $S_k[n]$ and $I_k[n]$ are expressed as (38) and (39) at the top of this page. (40) shows the inter-user interference power summation at the top of the next page, where $\mathbf{Z}_{mk,d} = \mathbf{R}_{mk}^d (\mathbf{\Psi}_{mk}^d)^{-1}$, $\mathbf{Z}_{mk,c} = \mathbf{R}_{mk}^c (\mathbf{\Psi}_{mk}^c)^{-1}$, $\forall m, \forall k$. Meanwhile, the EMI power is given by

$$\begin{aligned}
&\mathbb{E} \left\{ \left| \sum_{j=1}^J (\mathbf{\Phi}_j \mathbf{g}_{kj}^c[n])^T \mathbf{n}_j[n] \right|^2 \right\} \\
&= \sum_{j=1}^J \mathbb{E} \left\{ \left| (\mathbf{\Phi}_j \mathbf{g}_{kj}^c[n])^T \mathbf{n}_j[n] \right|^2 \right\} = \sum_{j=1}^J \beta_{kj} \sigma_j^2 \text{tr}(\mathbf{T}_j). \tag{41}
\end{aligned}$$

Proof: Please refer to Appendix A.

C. Sum SE Maximization

In this section, we provide the RIS coefficient matrix design to maximize the sum downlink SE. Note that the sum downlink SE depends on large-scale statistics, which experience slow variation since the distance variation is negligible compared with the initial distance. Thus, the proposed optimization problem can be performed across several coherence intervals [17]. To this end, the optimization problem of the RIS coefficient matrix can be formulated as

$$P_1 : \max_{\Theta} \text{SE}_{\text{sum}} = \sum_{k=1}^K \text{SE}_k \tag{42a}$$

subject to

$$|\mathbf{\Phi}_j(l, l)| = 1, \quad \forall l, \forall j, \tag{42b}$$

where $\Theta = [\mathbf{\Phi}_1, \dots, \mathbf{\Phi}_J] \in \mathbb{C}^{JL \times L}$. This optimization problem is non-convex [17], [33], [44], and to solve it in a suboptimal manner, we deploy the projected GA algorithm to obtain the local optimal solution of the maximization problem [17], [45]. For the proposed projected GA algorithm, increasing the objective from the current iteration $\mathbf{\Phi}_j^t$, $\forall j$ to the gradient direction, has the following iterations [44], [46], [47]

$$\mathbf{\Phi}_j^{t+1} = \mathbf{P}_{\mathbf{\Phi}_j} \left(\mathbf{\Phi}_j^t + \mu_j \nabla_{\mathbf{\Phi}_j} \text{SE}_{\text{sum}}(\mathbf{\Phi}^t) \right), \tag{43}$$

where μ_j is the step size for $\mathbf{\Phi}_j$, $\forall j$, and the superscript t is the iteration index. To meet the constraints, we apply the projection functions $\mathbf{P}_{\mathbf{\Phi}_j}(\mathbf{\Phi}_j)$ following [44]

$$[\mathbf{P}_{\mathbf{\Phi}_j}(\mathbf{\Phi}_j)]_{l,l} = \frac{\mathbf{\Phi}_j(l, l)}{|\mathbf{\Phi}_j(l, l)|}, \quad l = 1, \dots, L, \quad \forall j. \tag{44}$$

Note that, referring to [28], the complex gradients of $\text{SE}_{\text{sum}}(\Theta)$ in terms of $\mathbf{\Phi}_j$ can be computed as $\nabla_{\mathbf{\Phi}_j} \text{SE}_{\text{sum}}(\Theta)$

$$\begin{aligned}
& \sum_{k'=1}^K \mathbb{E} \left\{ \left| \sum_{m=1}^M \sqrt{\eta_{mk'}} \mathbf{g}_{mk'}^T [n] \hat{\mathbf{g}}_{mk'}^* [\lambda] \right|^2 \right\} \\
&= \sum_{k'=1}^K \sum_{m=1}^M \eta_{mk'} \text{tr} \left((\mathbf{Q}_{mk'}^d + \mathbf{Q}_{mk'}^c) \Delta_{mk} \right) \\
&+ \sum_{k' \in \mathcal{P}_k^c} \sum_{m=1}^M \eta_{mk'} \rho_k^2 [n - \lambda] p_p \rho_k^2 [\lambda - t_k^c] \sum_{j=1}^J \beta_{mj}^2 \beta_{kj}^2 \text{tr}(\mathbf{T}_j^2) \text{tr}(\mathbf{R}_{mj,r} \mathbf{Z}_{mk',c} \mathbf{R}_{mj,r} \mathbf{Z}_{mk',c}^H) \\
&+ \sum_{k'=1}^K \sum_{m=1}^M \sum_{m'=1}^M \sqrt{\eta_{mk'} \eta_{m'k'}} \sum_{j=1}^J \left(\sum_{k'' \in \mathcal{P}_{k'}} p_p \beta_{k''j} + \sigma_j^2 \right) \beta_{mj} \beta_{m'j} \beta_{kj} \text{tr}(\mathbf{T}_j^2) \text{tr}(\mathbf{R}_{mj,r} \mathbf{Z}_{mk',c} \mathbf{R}_{m'j,r} \mathbf{Z}_{m'k',c}^H) \\
&+ \sum_{k' \in \mathcal{P}_k^d \cap \mathcal{P}_k^c} \sum_{m=1}^M \sum_{m'=1}^M \sqrt{\eta_{mk'} \eta_{m'k'}} \rho_k^2 [n - \lambda] p_p \rho_k [\lambda - t_k^d] \rho_k [\lambda - t_k^c] \left(\text{tr}(\Delta_{mk}^d \mathbf{Z}_{mk',d}) \text{tr}(\Delta_{m'k}^c \mathbf{Z}_{m'k',c}^H) \right. \\
&\quad \left. + \text{tr}(\Delta_{mk}^c \mathbf{Z}_{mk',c}) \text{tr}(\Delta_{m'k}^d \mathbf{Z}_{m'k',d}^H) \right) \\
&+ \sum_{k' \in \mathcal{P}_k^d} \sum_{m=1}^M \sum_{m'=1}^M \sqrt{\eta_{mk'} \eta_{m'k'}} \rho_k^2 [n - \lambda] p_p \rho_k^2 [\lambda - t_k^d] \text{tr}(\Delta_{mk}^d \mathbf{Z}_{mk',d}) \text{tr}(\Delta_{m'k}^d \mathbf{Z}_{m'k',d}^H) \\
&+ \sum_{k' \in \mathcal{P}_k^c} \sum_{m=1}^M \sum_{m'=1}^M \sqrt{\eta_{mk'} \eta_{m'k'}} \rho_k^2 [n - \lambda] p_p \rho_k^2 [\lambda - t_k^c] \text{tr}(\Delta_{mk}^c \mathbf{Z}_{mk',c}) \text{tr}(\Delta_{m'k}^c \mathbf{Z}_{m'k',c}^H).
\end{aligned} \tag{40}$$

$$\begin{aligned}
\nabla_{\Phi_j} S_k [n] &= p_d \rho_k^2 [n - \lambda] \nabla_{\Phi_j} \left(\left| \sum_{m=1}^M \sqrt{\eta_{mk}} \text{tr}(\mathbf{Q}_{mk}^d + \mathbf{Q}_{mk}^c) \right|^2 \right) \\
&= p_d \rho_k^2 [n - \lambda] \sum_{m=1}^M \sum_{m'=1}^M \sqrt{\eta_{mk} \eta_{m'k}} \left(\text{tr}(\mathbf{Q}_{mk}^d + \mathbf{Q}_{m'k}^c) \nabla_{\Phi_j} \text{tr}(\mathbf{Q}_{mk}^c) + \text{tr}(\mathbf{Q}_{mk}^d + \mathbf{Q}_{mk}^c) \nabla_{\Phi_j} \text{tr}(\mathbf{Q}_{m'k}^c) \right) \\
&- p_d \rho_k^2 [n - \lambda] \sum_{m=1}^M \sum_{m'=1}^M \eta_{mk} \eta_{m'k} \text{tr}(\mathbf{Q}_{m'k}^d + \mathbf{Q}_{m'k}^c) \text{tr}(\mathbf{Q}_{mk}^d + \mathbf{Q}_{mk}^c) \nabla_{\Phi_j} \left(\frac{1}{\sqrt{\eta_{mk} \eta_{m'k}}} \right),
\end{aligned} \tag{46}$$

with the decomposition as

$$\begin{aligned}
\nabla_{\Phi_j} \text{SE}_{\text{sum}}(\Theta) &= \nabla_{\Phi_j} \sum_{k=1}^K \sum_{n=\lambda}^{\tau_c} \log_2 \left(1 + \frac{S_k [n]}{I_k [n]} \right) \\
&= \sum_{k=1}^K \sum_{n=\lambda}^{\tau_c} \frac{(\nabla_{\Phi_j} S_k [n]) I_k [n] - S_k [n] \nabla_{\Phi_j} I_k [n]}{\ln 2 I_k^2 [n] (1 + \frac{S_k [n]}{I_k [n]})}.
\end{aligned} \tag{45}$$

According to [48], [49], we can introduce the closed-form expressions of $\nabla_{\Phi_j} S_k [n]$ as (46) at the top of this page with

$$\nabla_{\Phi_j} \left(\frac{1}{\sqrt{\eta_{mk} \eta_{m'k}}} \right) = \frac{1}{2} \left(\begin{aligned} & \sqrt{\frac{\eta_{mk}}{\eta_{m'k}}} \sum_{k'=1}^K \nabla_{\Phi_j} \text{tr}(\mathbf{Q}_{mk'}^c) \\ & + \sqrt{\frac{\eta_{m'k}}{\eta_{mk}}} \sum_{k'=1}^K \nabla_{\Phi_j} \text{tr}(\mathbf{Q}_{m'k'}^c) \end{aligned} \right). \tag{47}$$

Meanwhile, $\nabla_{\Phi_j} I_k [n]$ are given by (48)-(51) at the top of the following pages. Based on the above-mentioned observations, Algorithm 1 delivers the iterative procedure of the projected GA algorithm to converge to a stationary point of P_1 [44]. We initialize the step size μ_j , $\forall j$, and reduce it by increasing the iterations. Note that we introduce the suitable step size at each iteration based on $\nabla_{\Phi_j} \text{SE}_{\text{sum}}(\Theta)$ for each RIS to further improve the performance of the projected GA algorithm.

Proof: Please refer to Appendix B.

V. NUMERICAL RESULTS

We shall consider a simulation setup with APs, users and RISs located within a geographic area of $D \times D$ km², where $D = 0.5$ km. Referring to [26], APs and users/RISs are randomly and independently distributed in two adjacent sub-regions with $x^{\text{AP}}, y^{\text{AP}} \in [-\frac{D}{2}, 0]$ km, $x^{\text{user}}, y^{\text{user}} \in [0, \frac{D}{2}]$ km and $x^{\text{RIS}}, y^{\text{RIS}} \in [0, \frac{D}{2}]$ km. $\beta_x = \text{PL}_x \cdot z_x$ ($x = mk, mj, kj$) models the large-scale fading coefficients. PL_x is the three-slope path loss and z_x is log-normal shadowing with the

Algorithm 1 Projected GA Algorithm Based RIS Design

Inputs: ϵ (tolerance), IterMax;

Output: Φ_j , $\forall j$, $\text{SE}_{\text{sum}}(\Theta)$

- 1: Initialize Φ_j^0 , $\mathbf{f}^0 = \text{SE}_{\text{sum}}(\Theta^0)$, $\forall j$
- 2: **for** $i = 1 : \text{IterMax}$ **do**
- 3: $\Phi_j = []$, $\forall j$
- 4: $\mu_j = (1 - \frac{i-1}{2 \cdot \text{IterMax}}) / |\nabla_{\Phi_j^0} \text{SE}(\Theta^0)|$; (step size)
- 5: $\Phi_j = \text{P}_{\Phi_j} \left(\Phi_j^0 + \mu_j \nabla_{\Phi_j^0} \text{SE}_{\text{sum}}(\Theta^0) \right)$, $\forall j$
- 6: Calculate $\mathbf{f} = \text{SE}_{\text{sum}}(\Theta)$, $\forall j$
- 7: **if** $|\mathbf{f} - \mathbf{f}^0| \leq \epsilon$ **then**
- 8: **break**
- 9: **else**
- 10: $\Phi_j^0 = \Phi_j$, $\mathbf{f}^0 = \mathbf{f}$, $\forall j$;
- 11: **end if**
- 12: **end for**

standard deviation σ_{sh} [1]. Likewise, $d_0 = 10$ m, $d_1 = 50$ m and $\sigma_{\text{sh}} = 8$ dB. The AP, RIS and user heights are 15 m, 30 m and 1.65 m [5]. Moreover, the exponential correlation model in [31], [50] is utilized for the spatial correlation of APs. Unless otherwise stated, all users experience the same velocity, $v_k = v$, $\forall k$. The pilot sequence length is $\tau_p = 3$, the carrier frequency equals $f_c = 1.9$ GHz, the bandwidth equals $B = 20$ MHz, the time instant length equals $T_s = 0.01$ ms. We also set downlink power as $p_d = 23$ dBm, pilot and uplink power as $p_p = p_u = 20$ dBm and $\sigma^2 = -91$ dBm [27]. We assume that all RIS elements provide $d_h = d_v = \lambda/4$ [2], [7]. For the projected GA algorithm, we set the maximum number of iterations IterMax= 20 and tolerance $\epsilon = 10^{-6}$ [47].

A. Channel Estimation Accuracy

The NMSEs of the proposed system versus p_p with different user velocities are shown in Fig. 2. For comparison, the

$$\begin{aligned}
\nabla_{\Phi_j} I_k[n] &= p_d \nabla_{\Phi_j} \left(\sum_{k'=1}^K \mathbb{E} \left\{ \left| \sum_{m=1}^M \sqrt{\eta_{mk'}} \mathbf{g}_{mk'}^T [n] \hat{\mathbf{g}}_{mk'}^* [\lambda] \right|^2 \right\} \right) - \nabla_{\Phi_j} S_k[n] + \nabla_{\Phi_j} \sum_{j=1}^J \beta_{kj} \sigma_j^2 \text{tr}(\mathbf{T}_j) \\
&= p_d \sum_{k'=1}^K \sum_{m=1}^M \eta_{mk'} \left(p_p \rho_k^2 [\lambda - t_k^c] \begin{bmatrix} \text{tr} \left((\Psi_{mk'}^c)^{-1} \Delta_{mk'}^c \Delta_{mk} \mathbf{\Pi}_{mk'j} \right) \\ + \text{tr} \left(\Delta_{mk} \Delta_{mk'}^c (\Psi_{mk'}^c)^{-1} \mathbf{\Pi}_{mk'j} \right) \\ - \sum_{k'' \in \mathcal{P}_{k'}^c} p_{k''}^c \text{tr} \left((\Psi_{mk'}^c)^{-1} \Delta_{mk'}^c \Delta_{mk} \Delta_{mk'}^c (\Psi_{mk'}^c)^{-1} \mathbf{\Pi}_{mk''j} \right) \\ - \beta_{mj} \sigma_j^2 \text{tr} \left((\Psi_{mk'}^c)^{-1} \Delta_{mk'}^c \Delta_{mk} \Delta_{mk'}^c (\Psi_{mk'}^c)^{-1} \mathbf{R}_{mj,r} \right) \end{bmatrix} + \text{tr} \left((\mathbf{Q}_{mk'}^d + \mathbf{Q}_{mk'}^c) \mathbf{\Pi}_{mk'j} \right) \right) \nabla_{\Phi_j} \text{tr}(\mathbf{T}_j) \\
&\quad - p_d \sum_{k'=1}^K \sum_{m=1}^M \eta_{mk'}^2 \text{tr} \left((\mathbf{Q}_{mk'}^d + \mathbf{Q}_{mk'}^c) \Delta_{mk} \right) \sum_{k''=1}^K \nabla_{\Phi_j} \text{tr}(\mathbf{Q}_{mk''}^c) \\
&\quad + p_d \sum_{k' \in \mathcal{P}_k^c} \sum_{m=1}^M \eta_{mk'} \rho_k^2 [n - \lambda] p_p \rho_k^2 [\lambda - t_k^c] \left(\begin{bmatrix} \beta_{mj}^2 \beta_{kj}^2 \text{tr} \left(\mathbf{R}_{mj,r} \mathbf{Z}_{mk',c} \mathbf{R}_{mj,r} \mathbf{Z}_{mk',c}^H \right) \cdot 2A_j^2 \text{diag} \left(\mathbf{R}_j^T \Phi_j^* \mathbf{R}_j^T \mathbf{T}_j^T \right) \\ + \sum_{j'=1}^J \beta_{mj'}^2 \beta_{kj'}^2 \text{tr}(\mathbf{T}_{j'}) \sqrt{p_p} \rho_k [\lambda - t_k^c] \mathbf{\Gamma}_{mmk'j'} \nabla_{\Phi_j} \text{tr}(\mathbf{T}_j) \end{bmatrix} \right) \\
&\quad - p_d \sum_{k' \in \mathcal{P}_k^c} \sum_{m=1}^M \eta_{mk'}^2 \rho_k^2 [n - \lambda] p_p \rho_k^2 [\lambda - t_k^c] \sum_{j=1}^J \beta_{mj}^2 \beta_{kj}^2 \text{tr}(\mathbf{T}_j^2) \text{tr} \left(\mathbf{R}_{mj,r} \mathbf{Z}_{mk',c} \mathbf{R}_{mj,r} \mathbf{Z}_{mk',c}^H \right) \sum_{k''=1}^K \nabla_{\Phi_j} \text{tr}(\mathbf{Q}_{mk''}^c) \\
&\quad + p_d \sum_{k'=1}^K \sum_{m=1}^M \sum_{m'=1}^M \sqrt{\eta_{mk'} \eta_{m'k'}} \left(\begin{bmatrix} \left(\sum_{k'' \in \mathcal{P}_{k'}^c} p_p \beta_{k''j} + \sigma_j^2 \right) \beta_{mj} \beta_{m'j} \beta_{kj} \text{tr} \left(\mathbf{R}_{mj,r} \mathbf{Z}_{mk',c} \mathbf{R}_{m'j,r} \mathbf{Z}_{m'k',c}^H \right) \cdot 2A_j^2 \text{diag} \left(\mathbf{R}_j^T \Phi_j^* \mathbf{R}_j^T \mathbf{T}_j^T \right) \\ + \sum_{j'=1}^J \left(\sum_{k'' \in \mathcal{P}_{k'}^c} p_p \beta_{k''j'} + \sigma_j^2 \right) \beta_{mj'} \beta_{m'j'} \beta_{kj'} \text{tr}(\mathbf{T}_{j'}) \sqrt{p_p} \rho_k [\lambda - t_k^c] \mathbf{\Gamma}_{mm'k'j'} \nabla_{\Phi_j} \text{tr}(\mathbf{T}_j) \end{bmatrix} \right) \\
&\quad - p_d \sum_{k'=1}^K \sum_{m=1}^M \sum_{m'=1}^M \eta_{mk'} \eta_{m'k'} \sum_{j=1}^J \left(\sum_{k'' \in \mathcal{P}_{k'}^c} p_p \beta_{k''j} + \sigma_j^2 \right) \beta_{mj} \beta_{m'j} \beta_{kj} \text{tr}(\mathbf{T}_j^2) \text{tr} \left(\mathbf{R}_{mj,r} \mathbf{Z}_{mk',c} \mathbf{R}_{m'j,r} \mathbf{Z}_{m'k',c}^H \right) \nabla_{\Phi_j} \left(\frac{1}{\sqrt{\eta_{mk'} \eta_{m'k'}}} \right) \\
&\quad + p_d \sum_{k' \in \mathcal{P}_k^d \cap \mathcal{P}_k^c} \sum_{m=1}^M \sum_{m'=1}^M \sqrt{\eta_{mk'} \eta_{m'k'}} \rho_k^2 [n - \lambda] p_p \rho_k [\lambda - t_k^d] \rho_k [\lambda - t_k^c] \left(\begin{bmatrix} \text{tr}(\Delta_{mk}^d \mathbf{Z}_{mk',d}) \nabla_{\Phi_j} \left(\text{tr}(\Delta_{m'k}^c \mathbf{Z}_{m'k',c}^H) \right) \\ + \text{tr}(\Delta_{m'k}^d \mathbf{Z}_{m'k',d}^H) \nabla_{\Phi_j} \left(\text{tr}(\Delta_{mk}^c \mathbf{Z}_{mk',c}) \right) \end{bmatrix} \right) \\
&\quad - p_d \sum_{k' \in \mathcal{P}_k^d \cap \mathcal{P}_k^c} \sum_{m=1}^M \sum_{m'=1}^M \eta_{mk'} \eta_{m'k'} \rho_k^2 [n - \lambda] p_p \rho_k [\lambda - t_k^d] \rho_k [\lambda - t_k^c] \left(\begin{bmatrix} \text{tr}(\Delta_{mk}^d \mathbf{Z}_{mk',d}) \text{tr}(\Delta_{m'k}^c \mathbf{Z}_{m'k',c}^H) \\ + \text{tr}(\Delta_{m'k}^d \mathbf{Z}_{m'k',d}^H) \text{tr}(\Delta_{mk}^c \mathbf{Z}_{mk',c}) \end{bmatrix} \right) \nabla_{\Phi_j} \left(\frac{1}{\sqrt{\eta_{mk'} \eta_{m'k'}}} \right) \\
&\quad + p_d \sum_{k' \in \mathcal{P}_k^c} \sum_{m=1}^M \sum_{m'=1}^M \sqrt{\eta_{mk'} \eta_{m'k'}} \rho_k^2 [n - \lambda] p_p \rho_k^2 [\lambda - t_k^c] \left(\text{tr}(\Delta_{mk}^c \mathbf{Z}_{mk',c}) \nabla_{\Phi_j} \left(\text{tr}(\Delta_{m'k}^c \mathbf{Z}_{m'k',c}^H) \right) + \text{tr}(\Delta_{m'k}^c \mathbf{Z}_{m'k',c}^H) \nabla_{\Phi_j} \left(\text{tr}(\Delta_{mk}^c \mathbf{Z}_{mk',c}) \right) \right) \\
&\quad - p_d \sum_{k' \in \mathcal{P}_k^c} \sum_{m=1}^M \sum_{m'=1}^M \eta_{mk'} \eta_{m'k'} \rho_k^2 [n - \lambda] p_p \rho_k^2 [\lambda - t_k^c] \text{tr}(\Delta_{mk}^c \mathbf{Z}_{mk',c}) \text{tr}(\Delta_{m'k}^c \mathbf{Z}_{m'k',c}^H) \nabla_{\Phi_j} \left(\frac{1}{\sqrt{\eta_{mk'} \eta_{m'k'}}} \right) \\
&\quad - \nabla_{\Phi_j} S_k[n] + \beta_{kj} \sigma_j^2 \nabla_{\Phi_j} \text{tr}(\mathbf{T}_j), \tag{48}
\end{aligned}$$

$$\begin{aligned}
\mathbf{\Gamma}_{mm'k'j} &= \text{tr} \left((\Psi_{mk'}^c)^{-1} \mathbf{R}_{m'j,r} \mathbf{Z}_{m'k',c}^H \mathbf{R}_{mj,r} \mathbf{\Pi}_{mk'j} \right) + \text{tr} \left(\mathbf{R}_{m'j,r} \mathbf{Z}_{m'k',c} \mathbf{R}_{mj,r} (\Psi_{mk'}^c)^{-1} \mathbf{\Pi}_{mk'j} \right) \\
&\quad - \sum_{k'' \in \mathcal{P}_{k'}^c} p_p \text{tr} \left((\Psi_{mk'}^c)^{-1} \mathbf{R}_{m'j',r} \mathbf{Z}_{m'k',c}^H \mathbf{R}_{mj',r} \Delta_{mk'}^c (\Psi_{mk'}^c)^{-1} \mathbf{\Pi}_{mk''j} \right) - \beta_{mj} \sigma_j^2 \text{tr} \left((\Psi_{mk'}^c)^{-1} \mathbf{R}_{m'j',r} \mathbf{Z}_{m'k',c}^H \mathbf{R}_{mj',r} \Delta_{mk'}^c (\Psi_{mk'}^c)^{-1} \mathbf{R}_{mj,r} \right) \\
&\quad - \sum_{k'' \in \mathcal{P}_{k'}^c} p_p \text{tr} \left((\Psi_{m'k'}^c)^{-1} \Delta_{m'k'}^c \mathbf{R}_{m'j',r} \mathbf{Z}_{m'k',c} \mathbf{R}_{m'j',r} (\Psi_{m'k'}^c)^{-1} \mathbf{\Pi}_{m'k''j} \right) - \beta_{mj} \sigma_j^2 \text{tr} \left((\Psi_{m'k'}^c)^{-1} \Delta_{m'k'}^c \mathbf{R}_{m'j',r} \mathbf{Z}_{m'k',c} \mathbf{R}_{m'j',r} (\Psi_{m'k'}^c)^{-1} \mathbf{R}_{m'j,r} \right), \tag{49}
\end{aligned}$$

$$\nabla_{\Phi_j} \left(\text{tr}(\Delta_{mk}^c \mathbf{Z}_{mk',c}^H) \right) = \text{tr}(\mathbf{Z}_{mk',c}^H \mathbf{\Pi}_{mk'j}) \nabla_{\Phi_j} \text{tr}(\mathbf{T}_j) + \sqrt{p_p} \rho_k [\lambda - t_k^c] \begin{bmatrix} \text{tr} \left(\Delta_{mk}^c (\Psi_{mk'}^c)^{-1} \mathbf{\Pi}_{mk'j} \right) \\ - \sum_{k'' \in \mathcal{P}_{k'}^c} p_p \text{tr} \left((\Psi_{mk'}^c)^{-1} \Delta_{mk'}^c \Delta_{mk}^c (\Psi_{mk'}^c)^{-1} \mathbf{\Pi}_{mk''j} \right) \\ - \beta_{mj} \sigma_j^2 \text{tr} \left((\Psi_{mk'}^c)^{-1} \Delta_{mk'}^c \Delta_{mk}^c (\Psi_{mk'}^c)^{-1} \mathbf{R}_{mj,r} \right) \end{bmatrix} \nabla_{\Phi_j} \text{tr}(\mathbf{T}_j), \tag{50}$$

conventional MMSE scheme with randomly assigned pilots, which estimates the aggregate channels simultaneously, shall serve as the benchmark scheme [7], [17], [36]. Meanwhile, the pilot length for the benchmark scheme is τ_p . The analytical

closed-form expressions generated by (21)-(22), (28)-(29) and (30)-(31) closely match the Monte Carlo (MC) simulations. It shows that our novel two-phase channel estimation scheme improves the accuracy of the estimation, giving a lower NMSE

$$\nabla_{\Phi_j} \left(\text{tr}(\Delta_{mk}^c \mathbf{Z}_{mk',c}) \right) = \text{tr}(\mathbf{Z}_{mk',c} \mathbf{\Pi}_{mkj}) \nabla_{\Phi_j} \text{tr}(\mathbf{T}_j) + \sqrt{p_p} \rho_{k'} [\lambda - t_{k'}^c] \begin{bmatrix} \text{tr} \left((\Psi_{mk'}^c)^{-1} \Delta_{mk}^c \mathbf{\Pi}_{mk'j} \right) \\ - \sum_{k'' \in \mathcal{P}_{k'}} p_p \text{tr} \left((\Psi_{mk'}^c)^{-1} \Delta_{mk}^c \Delta_{mk'}^c (\Psi_{mk'}^c)^{-1} \mathbf{\Pi}_{mk''j} \right) \\ - \beta_{mj} \sigma_j^2 \text{tr} \left((\Psi_{mk'}^c)^{-1} \Delta_{mk}^c \Delta_{mk'}^c (\Psi_{mk'}^c)^{-1} \mathbf{R}_{m,j,r} \right) \end{bmatrix} \nabla_{\Phi_j} \text{tr}(\mathbf{T}_j). \quad (51)$$

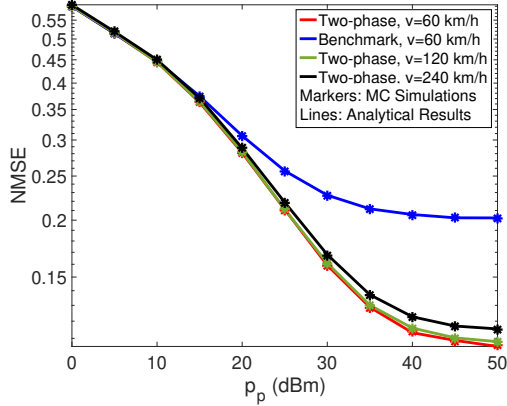


Fig. 2. NMSE vs p_p with $\zeta = 20$ dB, $M = 10$, $N = 2$, $K = 10$, $J = 4$, $L = 16$.

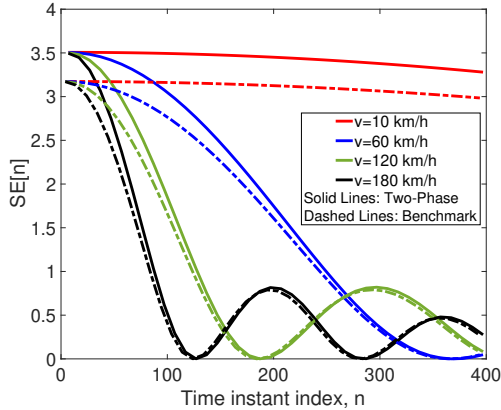


Fig. 3. SE vs the time instant index with $\zeta = 20$ dB, $M = 10$, $N = 2$, $K = 10$, $J = 4$, $L = 16$.

when pilot resources are limited. For example, when $v = 60$ km/h and $p_p = 20$ dBm, the two-phase scheme achieves a nearly 3%-likely improvement in NMSE than the benchmark scheme, and the improvement trend grows up to around 90%-likely improvement when $p_p = 50$ dBm. In this case, the proposed two-phase scheme can bloom its benefits with larger pilot power. Note that $\tau_p = 3 < K$ introduces pilot contamination, and EMI diminishes estimation accuracy. Thus, a non-zero error floor appears as p_p increases. Moreover, increasing user velocity contributes to greater channel aging effects and reduces temporal correlation coefficients, further degrading estimation accuracy. These results indicate that the two-phase estimation scheme significantly improves channel estimation accuracy, outperforming the benchmark scheme.

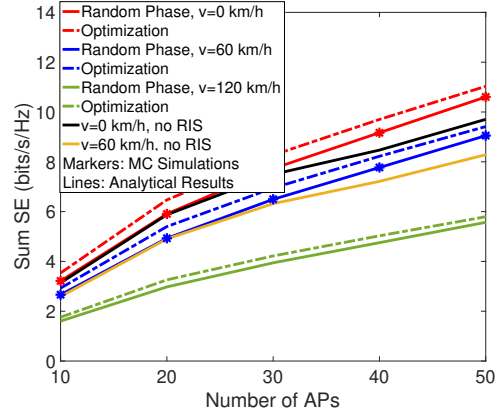


Fig. 4. Sum SE vs the number of APs with $\zeta = 20$ dB, $N = 2$, $K = 10$, $J = 4$, $L = 16$.

B. Channel Aging-aware Resource Block Length

Fig. 3 shows the downlink $\text{SE}[n] = \sum_{k=1}^K \log_2(1 + \text{SINR}_k[n])$ at n -th time instant regarding the first 400 time instant index. The downlink data transmission for the proposed two-phase scheme starts at $n = 2\tau_p + 1$, while the benchmark scheme starts at $n = \tau_p + 1$. Although the two-phase scheme exhibits a reduced transmission efficiency compared to the benchmark scheme by $(\tau_c - 2\tau_p)/(\tau_c - \tau_p)$, the results reveal that the proposed two-phase scheme outperforms the benchmark scheme at each time instant. We can also find that the two-phase scheme can achieve a nearly 10%-likely SE improvement compared to the benchmark scheme. As the temporal correlation coefficient diminishes with increasing time instant index, $\text{SE}[n]$ decreases. Meanwhile, the first zero position shifts leftward with higher user velocity, and the fluctuation peak becomes smaller with increasing time instant index. Therefore, selecting a reasonable resource block length is essential to mitigate channel aging effects. In the following, we select τ_c not to exceed the first zero index value at $v = 120$ km/h. As such, we consider $\tau_c = 196$, and all users are assumed to have the same velocity $v \leq 120$ km/h.

C. Spectral Efficiency Analysis

Fig. 4 depicts the sum SE, denoted as $\text{SE}_{\text{sum}} = \sum_{k=1}^K \text{SE}_k$, versus the number of APs and Fig. 5 shows the average SE per user, denoted as $\text{SE}_{\text{ave}} = \sum_{k=1}^K \text{SE}_k / K$ as a function of the number of antennas per AP. Different user velocities and number of users are evaluated. For comparison, the RIS-free cell-free massive MIMO system utilizes the benchmark channel estimation scheme outlined in this work. In Fig. 4, the analytical closed-form expressions generated by (36)-(41) can closely match the MC simulations. The results reveal

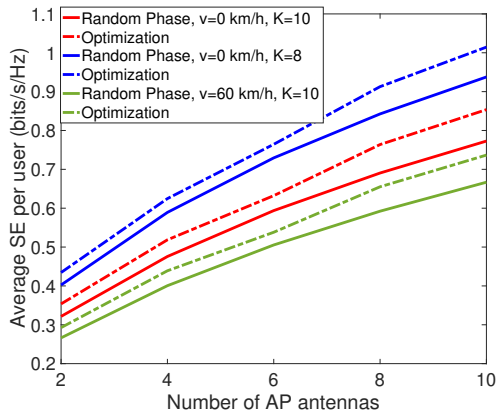


Fig. 5. Average SE vs the number of antennas per AP with $\zeta = 20$ dB, $M = 10$, $J = 4$, $L = 16$.

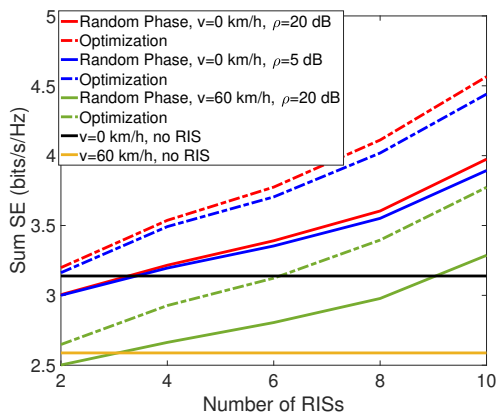


Fig. 6. Sum SE vs the number of RIS with $M = 10$, $N = 2$, $K = 10$, $L = 16$.

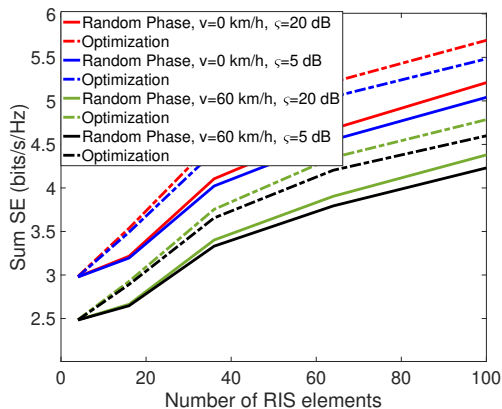


Fig. 7. Sum SE vs the number of elements per RIS with $M = 10$, $N = 2$, $K = 10$, $J = 4$.

that increasing the number of APs and antennas per AP can enhance spatial degrees of freedom to facilitate more efficient beamforming; therefore, the sum SE can be improved. In Fig. 4, the sum downlink SE optimized by the proposed projected GA algorithm exhibits over a 5% ~ 10%-likely SE improvement than that with the random RIS phases. Moreover, increasing APs can compensate for the performance

degradation caused by channel aging and EMI since increasing APs can achieve an SINR increase nearly proportional to it. Fig. 5 indicates that the sum SE achieved by the proposed projected GA algorithm surpasses that with random RIS phases by approximately 10% when $M = 4$. However, increasing the number of users may diminish average performance since more users introduce intensified pilot contamination and inter-user interference. Note that increasing the number of AP antennas can alleviate this decrease. Although EMI and channel aging introduce SE degradation, the proposed RIS-assisted system outperforms RIS-free cell-free massive MIMO systems, introducing a nearly 10%-likely SE improvement. In this case, integrating RISs into cell-free massive MIMO systems is advantageous. Meanwhile, an appropriate increase in the number of APs and antennas per AP is required to enhance system performance.

Fig. 6 and Fig. 7 illustrate the sum SE as a function of the number of RISs and the number of elements per RIS, respectively. Increasing the number of RISs and elements per RIS can effectively neutralize the performance degradation caused by channel aging and moderate EMI. For example, the proposed system achieves a notable SE improvement of 25% when $\zeta = 20$ dB and $J = 10$ compared to the benchmark RIS-free cell-free massive MIMO system. Passive beamforming and proper RIS configuration can improve interference management to release the necessity of introducing RISs and finding the RIS settings. Compared to the random RIS phases, the proposed projected GA algorithm can yield an extra 10% ~ 15%-likely SE improvement with an increasing number of RISs. Similarly, it can introduce a nearly 10%-likely SE improvement with an increasing number of RIS elements. These results underscore the effectiveness of the RIS coefficient matrix optimization algorithm in improving RIS-assisted system performance. However, under severe EMI conditions, i.e., $\zeta = 5$ dB, the proposed system struggles to deliver effective performance improvements, as the increased RISs and RIS elements exacerbate EMI to reduce system performance improvement. The result shows that EMI is non-negligible, and introducing EMI elimination schemes is necessary to further reap the benefits of deploying RISs. Despite the adverse effects of severe EMI, the advantages of incorporating RISs into cell-free massive MIMO systems remain substantial, and the RIS coefficient matrix design is necessary to compensate for the performance reduction caused by EMI.

VI. CONCLUSION

This paper analyzed the performance of RIS-assisted cell-free massive MIMO systems experiencing channel aging and EMI. To our knowledge, this work is the first to establish the system model for spatially correlated RIS-assisted cell-free massive MIMO systems with the joint effect of channel aging and EMI. Furthermore, it provides analytical expressions for downlink SE performance analysis. We applied a novel two-phase estimation scheme to mitigate the effects of channel aging and EMI. We adopted the downlink conjugate beamforming with fractional power control for performance

$$\begin{aligned}
T_1 &= \mathbf{g}_{mk}^T[\lambda] \hat{\mathbf{g}}_{mk'}^*[\lambda] \hat{\mathbf{g}}_{mk'}^T[\lambda] \mathbf{g}_{mk}^*[\lambda] = \mathbf{g}_{mk}^H[\lambda] \left(\hat{\mathbf{g}}_{mk'}^d[\lambda] + \hat{\mathbf{g}}_{mk'}^c[\lambda] \right)^H \left(\hat{\mathbf{g}}_{mk'}^d[\lambda] + \hat{\mathbf{g}}_{mk'}^c[\lambda] \right) \mathbf{g}_{mk}[\lambda] \\
&= \text{tr}(\Delta_{mk} \mathbf{Q}_{mk'}^c) + \text{tr}(\mathbf{Q}_{mk'}^d \Delta_{mk}) + \underbrace{p_p \rho_k^2 [\lambda - t_k^d] \text{tr}(\Delta_{mk}^d \mathbf{Z}_{mk',d}) \text{tr}(\Delta_{mk}^d \mathbf{Z}_{mk',d}^H)}_{k' \in \mathcal{P}_k^d} \\
&\quad + \underbrace{p_p \rho_k [\lambda - t_k^d] \rho_k [\lambda - t_k^c] \left(\text{tr}(\Delta_{mk}^d \mathbf{Z}_{mk',d}) \text{tr}(\Delta_{mk}^c \mathbf{Z}_{mk',c}^H) + \text{tr}(\Delta_{mk}^c \mathbf{Z}_{mk',c}) \text{tr}(\Delta_{mk}^d \mathbf{Z}_{mk',d}^H) \right)}_{k' \in \mathcal{P}_k^d \cap \mathcal{P}_k^c} \\
&\quad + \sum_{k'' \in \mathcal{P}_{k'}} p_p \sum_{j=1}^J \beta_{mj}^2 \beta_{kj} \beta_{k''j} \text{tr}(\mathbf{T}_j^2) \text{tr}(\mathbf{R}_{m,j,r} \mathbf{Z}_{mk',c}^H) \text{tr}(\mathbf{R}_{m,j,r} \mathbf{Z}_{mk',c}^H) + \sum_{j=1}^J \beta_{mj}^2 \beta_{kj} \sigma_j^2 \text{tr}(\mathbf{T}_j^2) \text{tr}(\mathbf{R}_{m,j,r} \mathbf{Z}_{mk',c}^H) \text{tr}(\mathbf{R}_{m,j,r} \mathbf{Z}_{mk',c}^H) \\
&\quad + \underbrace{p_p \rho_k^2 [\lambda - t_k^c] \left(\text{tr}(\Delta_{mk}^c \mathbf{Z}_{mk',c}) \text{tr}(\Delta_{mk}^c \mathbf{Z}_{mk',c}^H) + \sum_{j=1}^J \beta_{mj}^2 \beta_{kj}^2 \text{tr}(\mathbf{T}_j^2) \text{tr}(\mathbf{R}_{m,j,r} \mathbf{Z}_{mk',c} \mathbf{R}_{m,j,r} \mathbf{Z}_{mk',c}^H) \right)}_{k' \in \mathcal{P}_k^c},
\end{aligned} \tag{55}$$

improvement, deriving closed-form expressions for downlink SE. Subsequently, we utilized the closed-form expressions to maximize the sum SE with respect to the RIS coefficient matrices via the projected GA algorithm. It was shown that our novel two-phase channel estimation scheme could reduce the performance degradation caused by channel aging and EMI. Meanwhile, the proposed RIS coefficient matrix optimization could also alleviate performance degradation. However, the benefits of introducing more RISs and RIS elements could be diminished in environments with severe EMI, posing challenges for effective deployment.

APPENDIX A

DERIVATION OF UPLINK SE APPROXIMATIONS

This appendix provides the detailed derivation of $\text{SINR}_k[n]$ by using the UatF bound [12], [51] to obtain the SE of k -th user in (37). According to the MMSE properties, the estimate $\hat{\mathbf{g}}_{mk}[\lambda]$ and estimation error $\tilde{\mathbf{g}}_{mk}[\lambda]$ are uncorrelated [17]. The users in the same set, $k' \in \mathcal{P}_k^x$, $x = c, d$, share the same pilot sequence and $\tilde{\mathbf{g}}_{mk'}[\lambda]$ is correlated with $\mathbf{g}_{mk}[\lambda]$. We can obtain the following derivations referring to [7], [36].

1) Compute $\mathbb{E}\{|S_k[n]|^2\}$: the desired signal is given by,

$$\begin{aligned}
\mathbb{E}\{|S_k[n]|^2\} &= \mathbb{E}\left\{ p_d \rho_k^2 [n - \lambda] \left| \sum_{m=1}^M \sqrt{\eta_{mk}} \mathbb{E}\left\{ \mathbf{g}_{mk}^T[\lambda] \hat{\mathbf{g}}_{mk}^*[\lambda] \right\} \right|^2 \right\} \\
&= p_d \rho_k^2 [n - \lambda] \left| \sum_{m=1}^M \sqrt{\eta_{mk}} \text{tr}(\mathbf{Q}_{mk}^d + \mathbf{Q}_{mk}^c) \right|^2.
\end{aligned} \tag{52}$$

2) Compute $\mathbb{E}\{|I_k[n]|^2\}$: We can first decompose the inter-user interference term as

$$\begin{aligned}
\mathbb{E}\{|UI_{kk'}[n]|^2\} &= p_d \mathbb{E}\left\{ \left| \sum_{m=1}^M \sqrt{\eta_{mk'}} \mathbf{g}_{mk'}^T[n] \hat{\mathbf{g}}_{mk'}^*[\lambda] \right|^2 \right\} \\
&= p_d \mathbb{E}\left\{ \sum_{m=1}^M \sum_{m'=1}^M \sqrt{\eta_{mk'} \eta_{m'k'}} \mathbf{g}_{mk'}^T[n] \hat{\mathbf{g}}_{mk'}^*[\lambda] \hat{\mathbf{g}}_{m'k'}^T[\lambda] \mathbf{g}_{m'k}^*[\lambda] \right\}.
\end{aligned} \tag{53}$$

We decompose (53) into two parts: $m = m'$ and $m \neq m'$. First, by utilizing (32), the procedure of $m = m'$ is shown as

$$\begin{aligned}
&\mathbb{E}\left\{ \sum_{m=1}^M \eta_{mk'} \mathbf{g}_{mk'}^T[n] \hat{\mathbf{g}}_{mk'}^*[\lambda] \hat{\mathbf{g}}_{mk'}^T[\lambda] \mathbf{g}_{mk'}^*[\lambda] \right\} \\
&= \mathbb{E}\left\{ \sum_{m=1}^M \eta_{mk'} \rho_k^2 [n - \lambda] \underbrace{\mathbf{g}_{mk'}^T[\lambda] \hat{\mathbf{g}}_{mk'}^*[\lambda] \hat{\mathbf{g}}_{mk'}^T[\lambda] \mathbf{g}_{mk'}^*[\lambda]}_{T_1} \right\} \\
&\quad + \mathbb{E}\left\{ \sum_{m=1}^M \eta_{mk'} \bar{\rho}_k^2 [n - \lambda] \underbrace{\mathbf{e}_{mk'}^T[n] \hat{\mathbf{g}}_{mk'}^*[\lambda] \hat{\mathbf{g}}_{mk'}^T[\lambda] \mathbf{e}_{mk'}^*[\lambda]}_{T_2} \right\}.
\end{aligned} \tag{54}$$

The relevant terms can be further described as (55) at the top of this page and (56) at the top of the next page. Similarly, the procedure for $m \neq m'$ can be simplified as (57) at the top of the next page. Then, we derive the relevant terms by (58) and (59) at the top of the next page. According to the above procedure, the proof is completed.

APPENDIX B

PROOF OF COMPLEX GRADIENTS

This appendix delivers the derivations of complex gradients $\nabla_{\Phi_j} \text{SE}_{\text{sum}}(\Phi)$ in (45) regarding Φ_j , $\forall j$. When considering $\text{tr}(\mathbf{T}_j)$, we can obtain

$$\begin{aligned}
d \text{tr}(\mathbf{T}_j) &= \text{tr}\left(d(A_j^2 \mathbf{R}_j^{1/2} \Phi_j \mathbf{R}_j \Phi_j^H \mathbf{R}_j^{1/2}) \right) \\
&= A_j^2 \text{tr}\left(\mathbf{R}_j \Phi_j^H \mathbf{R}_j d\Phi_j + (\mathbf{R}_j \Phi_j \mathbf{R}_j)^T d\Phi_j^* \right),
\end{aligned} \tag{60}$$

since Φ_j is a diagonal matrix, then so must $d\Phi_j$. With the help of [48], we can obtain

$$\nabla_{\Phi_j} \text{tr}(\mathbf{T}_j) = A_j^2 (\mathbf{R}_j \Phi_j^H \mathbf{R}_j)^T \circ \mathbf{I} = A_j^2 \text{diag}(\mathbf{R}_j^T \Phi_j^* \mathbf{R}_j^T). \tag{61}$$

Based on Δ_{mk}^c in (10) and Ψ_{mk}^c in (29), we can derive the differentials $d(\Delta_{mk}^c)$ and $d((\Psi_{mk}^c)^{-1})$ as follows. With respect to $d(\Delta_{mk}^c)$, we can obtain [48], [49]

$$d(\Delta_{mk}^c) = d\left(\sum_{j=1}^J \beta_{mj} \beta_{kj} \text{tr}(\mathbf{T}_j) \mathbf{R}_{m,j,r} \right) = \sum_{j=1}^J \mathbf{\Pi}_{mkj} d \text{tr}(\mathbf{T}_j), \tag{62}$$

where $\mathbf{\Pi}_{mkj} = \beta_{mj} \beta_{kj} \mathbf{R}_{m,j,r}$. By applying (60)-(61), we can have

$$\nabla_{\Phi_j} \text{tr}(\Delta_{mk}^c) = A_j^2 \beta_{mj} \beta_{kj} \text{tr}(\mathbf{R}_{m,j,r}) \text{diag}(\mathbf{R}_j^T \Phi_j^* \mathbf{R}_j^T). \tag{63}$$

Referring to [44], we can derive $d((\Psi_{mk}^c)^{-1})$ as

$$d((\Psi_{mk}^c)^{-1}) = -(\Psi_{mk}^c)^{-1} d(\Psi_{mk}^c) (\Psi_{mk}^c)^{-1}, \tag{64}$$

where $d(\Psi_{mk}^c)$ can be obtained by

$$\begin{aligned}
d(\Psi_{mk}^c) &= d\left(\sum_{k' \in \mathcal{P}_k^c} p_p \Delta_{mk'}^c + \sum_{j=1}^J \beta_{mj} \sigma_j^2 \text{tr}(\mathbf{T}_j) \mathbf{R}_{m,j,r} + \sigma^2 \mathbf{I}_N \right) \\
&= \sum_{k' \in \mathcal{P}_k^c} p_p d(\Delta_{mk'}^c) + \sum_{j=1}^J \beta_{mj} \sigma_j^2 d(\text{tr}(\mathbf{T}_j)) \mathbf{R}_{m,j,r},
\end{aligned} \tag{65}$$

Then, we can obtain $d(\mathbf{Q}_{mk}^c)$ as (66) and the differential of $\text{tr}(\mathbf{Q}_{mk}^c)$ as (67) at the top of the next page [44], [49]. Next,

$$\begin{aligned}
T_2 &= \mathbf{e}_{mk}^T [n] \hat{\mathbf{g}}_{mk'}^* [\lambda] \hat{\mathbf{g}}_{mk'}^T [\lambda] \mathbf{e}_{mk}^* [n] = \mathbf{e}_{mk}^H [n] \left(\hat{\mathbf{g}}_{mk'}^d [\lambda] + \hat{\mathbf{g}}_{mk'}^c [\lambda] \right)^H \left(\hat{\mathbf{g}}_{mk'}^d [\lambda] + \hat{\mathbf{g}}_{mk'}^c [\lambda] \right) \mathbf{e}_{mk} [n] \\
&= \text{tr}(\Delta_{mk} \mathbf{Q}_{mk'}^c) + \text{tr}(\mathbf{Q}_{mk'}^d \Delta_{mk}) \\
&\quad + \sum_{k'' \in \mathcal{P}_{k'}} p_p \sum_{j=1}^J \beta_{mj}^2 \beta_{kj} \beta_{k''j} \text{tr}(\mathbf{T}_j^2) \text{tr}(\mathbf{R}_{m,j,r} \mathbf{Z}_{mk',c}) \text{tr}(\mathbf{R}_{m,j,r} \mathbf{Z}_{mk',c}^H) + \sum_{j=1}^J \beta_{mj}^2 \beta_{kj} \sigma_j^2 \text{tr}(\mathbf{T}_j^2) \text{tr}(\mathbf{R}_{m,j,r} \mathbf{Z}_{mk',c}) \text{tr}(\mathbf{R}_{m,j,r} \mathbf{Z}_{mk',c}^H).
\end{aligned} \tag{56}$$

$$\begin{aligned}
\mathbb{E} \left\{ \sum_{m=1}^M \sum_{\substack{m'=1 \\ m' \neq m}}^M \sqrt{\eta_{mk'} \eta_{m'k'}} \mathbf{g}_{mk'}^T [n] \hat{\mathbf{g}}_{mk'}^* [\lambda] \hat{\mathbf{g}}_{m'k'}^T [\lambda] \mathbf{g}_{m'k}^* [n] \right\} &= \mathbb{E} \left\{ \sum_{m=1}^M \sum_{\substack{m'=1 \\ m' \neq m}}^M \sqrt{\eta_{mk'} \eta_{m'k'}} \rho_k^2 [n - \lambda] \underbrace{\mathbf{g}_{mk}^T [\lambda] \hat{\mathbf{g}}_{mk'}^* [\lambda] \hat{\mathbf{g}}_{m'k'}^T [\lambda] \mathbf{g}_{m'k}^* [n]}_{T_3} \right\} \\
&\quad + \mathbb{E} \left\{ \sum_{m=1}^M \sum_{\substack{m'=1 \\ m' \neq m}}^M \sqrt{\eta_{mk'} \eta_{m'k'}} \bar{\rho}_k^2 [n - \lambda] \underbrace{\mathbf{e}_{mk}^T [n] \hat{\mathbf{g}}_{mk'}^* [\lambda] \hat{\mathbf{g}}_{m'k'}^T [\lambda] \mathbf{e}_{m'k}^* [n]}_{T_4} \right\},
\end{aligned} \tag{57}$$

$$\begin{aligned}
T_3 &= \mathbf{g}_{mk}^T [\lambda] \hat{\mathbf{g}}_{mk'}^* [\lambda] \hat{\mathbf{g}}_{m'k'}^T [\lambda] \mathbf{g}_{m'k}^* [n] = \mathbf{g}_{mk}^H [\lambda] \left(\hat{\mathbf{g}}_{mk'}^d [\lambda] + \hat{\mathbf{g}}_{mk'}^c [\lambda] \right)^H \left(\hat{\mathbf{g}}_{m'k'}^d [\lambda] + \hat{\mathbf{g}}_{m'k'}^c [\lambda] \right) \mathbf{g}_{m'k} [n] \\
&= \underbrace{p_p \rho_k^2 [\lambda - t_k^d] \text{tr}(\Delta_{mk'}^d \mathbf{Z}_{mk',d}) \text{tr}(\Delta_{m'k'}^d \mathbf{Z}_{m'k',d}^H)}_{k' \in \mathcal{P}_k^d} + \underbrace{p_p \rho_k^2 [\lambda - t_k^c] \text{tr}(\Delta_{mk'}^c \mathbf{Z}_{mk',c}) \text{tr}(\Delta_{m'k'}^c \mathbf{Z}_{m'k',c}^H)}_{k' \in \mathcal{P}_k^c} \\
&\quad + \underbrace{p_p \rho_k [\lambda - t_k^d] \rho_k [\lambda - t_k^c] \left(\text{tr}(\Delta_{mk'}^d \mathbf{Z}_{mk',d}) \text{tr}(\Delta_{m'k'}^c \mathbf{Z}_{m'k',c}^H) + \text{tr}(\Delta_{mk'}^c \mathbf{Z}_{mk',c}) \text{tr}(\Delta_{m'k'}^d \mathbf{Z}_{m'k',d}^H) \right)}_{k' \in \mathcal{P}_k^d \cap \mathcal{P}_k^c} \\
&\quad + \sum_{k'' \in \mathcal{P}_{k'}} p_p \sum_{j=1}^J \beta_{mj} \beta_{m'j} \beta_{kj} \beta_{k''j} \text{tr}(\mathbf{T}_j^2) \text{tr}(\mathbf{R}_{m,j,r} \mathbf{Z}_{mk',c}) \text{tr}(\mathbf{R}_{m',j,r} \mathbf{Z}_{m'k',c}^H) + \sum_{j=1}^J \beta_{mj} \beta_{m'j} \beta_{kj} \sigma_j^2 \text{tr}(\mathbf{T}_j^2) \text{tr}(\mathbf{R}_{m,j,r} \mathbf{Z}_{mk',c}) \text{tr}(\mathbf{R}_{m',j,r} \mathbf{Z}_{m'k',c}^H),
\end{aligned} \tag{58}$$

$$\begin{aligned}
T_4 &= \mathbf{e}_{mk}^T [n] \hat{\mathbf{g}}_{mk'}^* [\lambda] \hat{\mathbf{g}}_{m'k'}^T [\lambda] \mathbf{e}_{m'k}^* [n] = \mathbf{e}_{mk}^H [n] \left(\hat{\mathbf{g}}_{mk'}^d [\lambda] + \hat{\mathbf{g}}_{mk'}^c [\lambda] \right)^H \left(\hat{\mathbf{g}}_{m'k'}^d [\lambda] + \hat{\mathbf{g}}_{m'k'}^c [\lambda] \right) \mathbf{e}_{m'k} [n] \\
&= \sum_{k'' \in \mathcal{P}_{k'}} p_p \sum_{j=1}^J \beta_{mj} \beta_{m'j} \beta_{kj} \beta_{k''j} \text{tr}(\mathbf{T}_j^2) \text{tr}(\mathbf{R}_{m,j,r} \mathbf{Z}_{mk',c}) \text{tr}(\mathbf{R}_{m',j,r} \mathbf{Z}_{m'k',c}^H) + \sum_{j=1}^J \beta_{mj} \beta_{m'j} \beta_{kj} \sigma_j^2 \text{tr}(\mathbf{T}_j^2) \text{tr}(\mathbf{R}_{m,j,r} \mathbf{Z}_{mk',c}) \text{tr}(\mathbf{R}_{m',j,r} \mathbf{Z}_{m'k',c}^H).
\end{aligned} \tag{59}$$

$$\begin{aligned}
d(\mathbf{Q}_{mk}^c) &= d(\mathbf{R}_{mk}^c (\Psi_{mk}^c)^{-1} \mathbf{R}_{mk}^c) = d(\mathbf{R}_{mk}^c) (\Psi_{mk}^c)^{-1} \mathbf{R}_{mk}^c + \mathbf{R}_{mk}^c d((\Psi_{mk}^c)^{-1}) \mathbf{R}_{mk}^c + \mathbf{R}_{mk}^c (\Psi_{mk}^c)^{-1} d(\mathbf{R}_{mk}^c) \\
&= d(\mathbf{R}_{mk}^c) (\Psi_{mk}^c)^{-1} \mathbf{R}_{mk}^c - \mathbf{R}_{mk}^c (\Psi_{mk}^c)^{-1} d(\Psi_{mk}^c) (\Psi_{mk}^c)^{-1} \mathbf{R}_{mk}^c + \mathbf{R}_{mk}^c (\Psi_{mk}^c)^{-1} d(\mathbf{R}_{mk}^c),
\end{aligned} \tag{66}$$

$$\begin{aligned}
d(\text{tr}(\mathbf{Q}_{mk}^c)) &= \text{tr}(d(\mathbf{Q}_{mk}^c)) = \text{tr} \left(d(\mathbf{R}_{mk}^c) (\Psi_{mk}^c)^{-1} \mathbf{R}_{mk}^c - \mathbf{R}_{mk}^c (\Psi_{mk}^c)^{-1} d(\Psi_{mk}^c) (\Psi_{mk}^c)^{-1} \mathbf{R}_{mk}^c + \mathbf{R}_{mk}^c (\Psi_{mk}^c)^{-1} d(\mathbf{R}_{mk}^c) \right) \\
&= p_p \rho_k^2 [\lambda - t_k^c] \text{tr} \left(d(\Delta_{mk}^c) (\Psi_{mk}^c)^{-1} \Delta_{mk}^c - \Delta_{mk}^c (\Psi_{mk}^c)^{-1} d(\Psi_{mk}^c) (\Psi_{mk}^c)^{-1} \Delta_{mk}^c + \Delta_{mk}^c (\Psi_{mk}^c)^{-1} d(\Delta_{mk}^c) \right) \\
&= p_p \rho_k^2 [\lambda - t_k^c] \left[\begin{array}{l} \sum_{j=1}^J \text{tr} \left((\Psi_{mk}^c)^{-1} \Delta_{mk}^c \mathbf{\Pi}_{mkj} \right) + \sum_{j=1}^J \text{tr} \left(\Delta_{mk}^c (\Psi_{mk}^c)^{-1} \mathbf{\Pi}_{mkj} \right) \\ - \sum_{j=1}^J \sum_{k'' \in \mathcal{P}_{k'}} p_p \text{tr} \left((\Psi_{mk}^c)^{-1} \Delta_{mk}^c \Delta_{mk}^c (\Psi_{mk}^c)^{-1} \mathbf{\Pi}_{mk'j} \right) \\ - \sum_{j=1}^J \beta_{mj} \sigma_j^2 \text{tr} \left((\Psi_{mk}^c)^{-1} \Delta_{mk}^c \Delta_{mk}^c (\Psi_{mk}^c)^{-1} \mathbf{R}_{m,j,r} \right) \end{array} \right] d\text{tr}(\mathbf{T}_j)
\end{aligned} \tag{67}$$

$$\begin{aligned}
\nabla_{\Phi_j} \text{tr}(\mathbf{Q}_{mk}^c) &= A_j^2 p_p \rho_k^2 [\lambda - t_k^c] \left[\begin{array}{l} \text{tr} \left((\Psi_{mk}^c)^{-1} \Delta_{mk}^c \mathbf{\Pi}_{mkj} \right) + \text{tr} \left(\Delta_{mk}^c (\Psi_{mk}^c)^{-1} \mathbf{\Pi}_{mkj} \right) \\ - \sum_{k'' \in \mathcal{P}_{k'}} p_p \text{tr} \left((\Psi_{mk}^c)^{-1} \Delta_{mk}^c \Delta_{mk}^c (\Psi_{mk}^c)^{-1} \mathbf{\Pi}_{mk'j} \right) \\ - \beta_{mj} \sigma_j^2 \text{tr} \left((\Psi_{mk}^c)^{-1} \Delta_{mk}^c \Delta_{mk}^c (\Psi_{mk}^c)^{-1} \mathbf{R}_{m,j,r} \right) \end{array} \right] \text{diag}(\mathbf{R}_j^T \Phi_j^* \mathbf{R}_j^T),
\end{aligned} \tag{68}$$

we can obtain the derivative $\nabla_{\Phi_j} \text{tr}(\mathbf{Q}_{mk}^c)$ as (68) at the top of this page. Similarly, we can obtain the derivative $\nabla_{\Phi_j} \text{tr}(\mathbf{Z}_{mk,c})$ as (69) at the top of the next page.

REFERENCES

- [1] H. Q. Ngo *et al.*, "Cell-free massive MIMO versus small cells," *IEEE Trans. Wireless Commun.*, vol. 16, no. 3, pp. 1834–1850, 2017.
- [2] T. Van Chien *et al.*, "Reconfigurable intelligent surface-assisted cell-free massive MIMO systems over spatially-correlated channels," *IEEE Trans. Wireless Commun.*, vol. 21, no. 7, pp. 5106–5128, 2022.
- [3] H. He *et al.*, "Cell-free massive MIMO for 6G wireless communication networks," *J. Commun. Net.*, vol. 6, no. 4, pp. 321–335, 2021.
- [4] K. B. Letaief *et al.*, "The roadmap to 6G: AI empowered wireless networks," *IEEE Commun. Mag.*, vol. 57, no. 8, pp. 84–90, 2019.
- [5] Y. Zhang *et al.*, "Performance analysis of RIS-assisted cell-free massive MIMO systems with transceiver hardware impairments," *IEEE Trans.*

$$\nabla_{\Phi_j} \text{tr}(\mathbf{Z}_{m_k,c}) = A_j^2 \sqrt{p_p} \rho_k [\lambda - t_k^c] \begin{bmatrix} \text{tr}((\Psi_{m_k}^c)^{-1} \mathbf{\Pi}_{m_k,j}) - \sum_{k' \in \mathcal{P}_k^c} p_{p'} \text{tr}((\Psi_{m_k}^c)^{-1} \Delta_{m_k}^c (\Psi_{m_k}^c)^{-1} \mathbf{\Pi}_{m_k',j}) \\ -\beta_{m_j} \sigma_j^2 \text{tr}((\Psi_{m_k}^c)^{-1} \Delta_{m_k}^c (\Psi_{m_k}^c)^{-1} \mathbf{R}_{m_j,r}) \end{bmatrix} \text{diag}(\mathbf{R}_j^T \Phi_j^* \mathbf{R}_j^T). \quad (69)$$

- Commun.*, pp. 1–1, 2023.
- [6] E. Björnson *et al.*, “Deploying dense networks for maximal energy efficiency: Small cells meet massive MIMO,” *IEEE J. Sel. Areas Commun.*, vol. 34, no. 4, pp. 832–847, 2016.
- [7] E. Shi *et al.*, “Uplink performance of RIS-aided cell-free massive MIMO system with electromagnetic interference,” *IEEE J. Sel. Areas Commun.*, vol. 41, no. 8, pp. 2431–2445, 2023.
- [8] —, “Spatially correlated reconfigurable intelligent surfaces-aided cell-free massive MIMO systems,” *IEEE Trans. Veh. Technol.*, vol. 71, no. 8, pp. 9073–9077, 2022.
- [9] J. Qian *et al.*, “The effect of spatial correlation and mutual coupling on cell-free massive MIMO,” in *Proc. IEEE WCNC*, 2024, pp. 01–06.
- [10] E. Nayebi *et al.*, “Precoding and power optimization in cell-free massive MIMO systems,” *IEEE Trans. Wireless Commun.*, vol. 16, no. 7, pp. 4445–4459, 2017.
- [11] G. Interdonato *et al.*, “Enhanced normalized conjugate beamforming for cell-free massive MIMO,” *IEEE Trans. Commun.*, vol. 69, no. 5, pp. 2863–2877, 2021.
- [12] J. Zheng *et al.*, “Impact of channel aging on cell-free massive MIMO over spatially correlated channels,” *IEEE Trans. Wireless Commun.*, vol. 20, no. 10, pp. 6451–6466, 2021.
- [13] E. Björnson and L. Sanguinetti, “Scalable cell-free massive MIMO systems,” *IEEE Trans. Commun.*, vol. 68, no. 7, pp. 4247–4261, 2020.
- [14] H. D. Tuan *et al.*, “Scalable user rate and energy-efficiency optimization in cell-free massive MIMO,” *IEEE Trans. Commun.*, vol. 70, no. 9, pp. 6050–6065, 2022.
- [15] Q. Wu *et al.*, “Intelligent reflecting surface-aided wireless communications: A tutorial,” *IEEE Trans. Commun.*, vol. 69, no. 5, pp. 3313–3351, 2021.
- [16] Y. Zhang *et al.*, “Channel aging-aware precoding for RIS-aided multi-user communications,” *IEEE Trans. Veh. Technol.*, vol. 72, no. 2, pp. 1997–2008, 2023.
- [17] A. Papazafeiropoulos *et al.*, “Impact of channel aging on reconfigurable intelligent surface aided massive MIMO systems with statistical CSI,” *IEEE Trans. Veh. Technol.*, vol. 72, no. 1, pp. 689–703, 2023.
- [18] Y. Zhang *et al.*, “Performance analysis of reconfigurable intelligent surface assisted systems under channel aging,” *Intelligent and Converged Networks*, vol. 3, no. 1, pp. 74–85, 2022.
- [19] A. de Jesus Torres *et al.*, “Electromagnetic interference in RIS-aided communications,” *IEEE Wireless Commun. Lett.*, vol. 11, no. 4, pp. 668–672, 2022.
- [20] A. Khaleel and E. Basar, “Electromagnetic interference cancellation for RIS-assisted communications,” *IEEE Commun. Lett.*, vol. 27, no. 8, pp. 2192–2196, 2023.
- [21] G. S. Chandra *et al.*, “Downlink URLLC system over spatially correlated RIS channels and electromagnetic interference,” *IEEE Wirel. Commun. Lett.*, vol. 11, no. 9, pp. 1950–1954, 2022.
- [22] S. Hassouna *et al.*, “Reconfigurable intelligent surfaces aided wireless communications with electromagnetic interference,” in *Proc. IEEE Eu-CAP*, 2023, pp. 1–5.
- [23] M. a. Bashar, “On the performance of reconfigurable intelligent surface-aided cell-free massive MIMO uplink,” in *Proc. IEEE GLOBECOM*, 2020, pp. 1–6.
- [24] N. T. Nguyen *et al.*, “Downlink throughput of cell-free massive MIMO systems assisted by hybrid relay-reflecting intelligent surfaces,” in *Proc. IEEE ICC*, 2022, pp. 1475–1480.
- [25] E. Shi *et al.*, “Uplink performance of RIS-aided cell-free massive MIMO system over spatially correlated channels,” in *Proc. IEEE GLOBECOM*, 2022, pp. 3259–3264.
- [26] J. Qian *et al.*, “Two-phase channel estimation for RIS-aided cell-free massive MIMO with electromagnetic interference,” in *Proc. IEEE MeditCom*, 2024, pp. 471–476.
- [27] X. Ma *et al.*, “Active STAR-RIS aided cell-free massive MIMO: A performance study,” *IEEE Trans. Veh. Technol.*, pp. 1–6, 2023.
- [28] Y. Lu *et al.*, “Performance analysis of RIS-assisted communications with hardware impairments and channel aging,” *IEEE Trans. Commun.*, vol. 72, no. 6, pp. 3720–3735, 2024.
- [29] E. Björnson *et al.*, “Optimal design of energy-efficient multi-user MIMO systems: Is massive MIMO the answer?” *IEEE Trans. Wireless Commun.*, vol. 14, no. 6, pp. 3059–3075, 2015.
- [30] D. Shen *et al.*, “Joint beamforming design for RIS-assisted cell-free network with multi-hop transmissions,” *Tsinghua Science and Technology*, vol. 28, no. 6, pp. 1115–1127, 2023.
- [31] X. Li *et al.*, “Massive MIMO with multi-antenna users: When are additional user antennas beneficial?” in *Proc. IEEE ICT*, 2016, pp. 1–6.
- [32] Ö. T. Demir and E. Björnson, “RIS-assisted massive MIMO with multi-specular spatially correlated fading,” in *Proc. IEEE GLOBECOM*, 2021, pp. 1–6.
- [33] J. Qian *et al.*, “Performance analysis of STAR-RIS-assisted cell-free massive MIMO systems with electromagnetic interference and phase errors,” 2024. [Online]. Available: <https://arxiv.org/abs/2411.14030>
- [34] E. Björnson and L. Sanguinetti, “Rayleigh fading modeling and channel hardening for reconfigurable intelligent surfaces,” *IEEE Wirel. Commun. Lett.*, vol. 10, no. 4, pp. 830–834, 2021.
- [35] J. Yao *et al.*, “Robust beamforming design for RIS-aided cell-free systems with CSI uncertainties and capacity-limited backhaul,” *IEEE Trans. Commun.*, vol. 71, no. 8, pp. 4636–4649, 2023.
- [36] E. Shi *et al.*, “RIS-aided cell-free massive MIMO systems with channel aging,” *IEEE Trans. Veh. Tech.*, pp. 1–16, 2024.
- [37] R. Chopra *et al.*, “Uplink performance analysis of cell-free mMIMO systems under channel aging,” *IEEE Commun. Lett.*, vol. 25, no. 7, pp. 2206–2210, 2021.
- [38] A. K. Papazafeiropoulos and T. Ratnarajah, “Deterministic equivalent performance analysis of time-varying massive MIMO systems,” *IEEE Trans. Wireless Commun.*, vol. 14, no. 10, pp. 5795–5809, 2015.
- [39] J. Qian *et al.*, “Partial CSI acquisition for size-constrained massive MIMO systems with user mobility,” *IEEE Trans. Veh. Technol.*, vol. 67, no. 9, pp. 9016–9020, 2018.
- [40] A. K. Papazafeiropoulos, “Impact of general channel aging conditions on the downlink performance of massive MIMO,” *IEEE Trans. Veh. Technol.*, vol. 66, no. 2, pp. 1428–1442, 2017.
- [41] J. Xu *et al.*, “Reconfiguring wireless environments via intelligent surfaces for 6G: reflection, modulation, and security,” *Sci. China Inf. Sci.*, vol. 66, no. 3, p. 130304, 2023.
- [42] J. Jose *et al.*, “Pilot contamination and precoding in multi-cell TDD systems,” *IEEE Trans. Wireless Commun.*, vol. 10, no. 8, pp. 2640–2651, 2011.
- [43] R. Nikbakht *et al.*, “Uplink fractional power control and downlink power allocation for cell-free networks,” *IEEE Wirel. Commun. Lett.*, vol. 9, no. 6, pp. 774–777, 2020.
- [44] A. Papazafeiropoulos *et al.*, “STAR-RIS assisted cell-free massive MIMO system under spatially-correlated channels,” *IEEE Trans. Veh. Tech.*, vol. 73, no. 3, pp. 3932–3948, 2024.
- [45] H. Ge *et al.*, “Impact of phase noise in downlink STAR-RIS-aided massive MIMO systems,” *IEEE Commun. Lett.*, vol. 28, no. 2, pp. 392–396, 2024.
- [46] A. Papazafeiropoulos *et al.*, “Cooperative RIS and STAR-RIS assisted mmimo communication: Analysis and optimization,” *IEEE Trans. Veh. Tech.*, vol. 72, no. 9, pp. 11975–11989, 2023.
- [47] R. Ranjan *et al.*, “A gradient ascent based low complexity rate maximization algorithm for intelligent reflecting surface-aided OFDM systems,” *IEEE Commun. Lett.*, vol. 27, no. 8, pp. 2083–2087, 2023.
- [48] T. P. Minka, “Old and new matrix algebra useful for statistics,” 2000. [Online]. Available: <https://api.semanticscholar.org/CorpusID:15971655>
- [49] A. Hjørungnes and D. Gesbert, “Complex-valued matrix differentiation: Techniques and key results,” *IEEE Trans. Signal Proc.*, vol. 55, no. 6, pp. 2740–2746, 2007.
- [50] S. Loyka, “Channel capacity of MIMO architecture using the exponential correlation matrix,” *IEEE Commun. Lett.*, vol. 5, no. 9, pp. 369–371, 2001.
- [51] E. Björnson and L. Sanguinetti, “Making cell-free massive MIMO competitive with MMSE processing and centralized implementation,” *IEEE Trans. Wireless Commun.*, vol. 19, no. 1, pp. 77–90, 2020.